Electronic Supplementary Material (ESI) for Inorganic Chemistry Frontiers.

Electronic Supplementary Material **(ESI)**

A concerted evolution of supramolecular interactions in a {cation; metal complex; π-acid; solvent} anion-π system

Emilia Kuzniak,[†] James Hooper,[†] Monika Srebro-Hooper,[†] Jedrzej Kobylarczyk,[†] Magdalena Dziurka,[†] Bogdan Musielak,[†] Dawid Pinkowicz,[†] Jesus Raya,[‡] Sylvie Ferlay,[§] and Robert Podgajny*[†]

†Faculty of Chemistry, Jagiellonian University, Gronostajowa 2, 30-387 Krakow, Poland.

‡ Membrane Biophysics and NMR, Institute of Chemistry, UMR 7177, University of Strasbourg, 67000 Strasbourg, France.

§ Université de Strasbourg, CNRS, CMC UMR 7140, F-67000 Strasbourg, France.

All figures and tables in the table of content and in whole text are linked directly with their exact location in the file. Please use CTRL + Left Mouse Button.

Table of content:

Figures:

Tables:

I. Crystallization and recrystallization

Selected details of crystallization and recrystallization

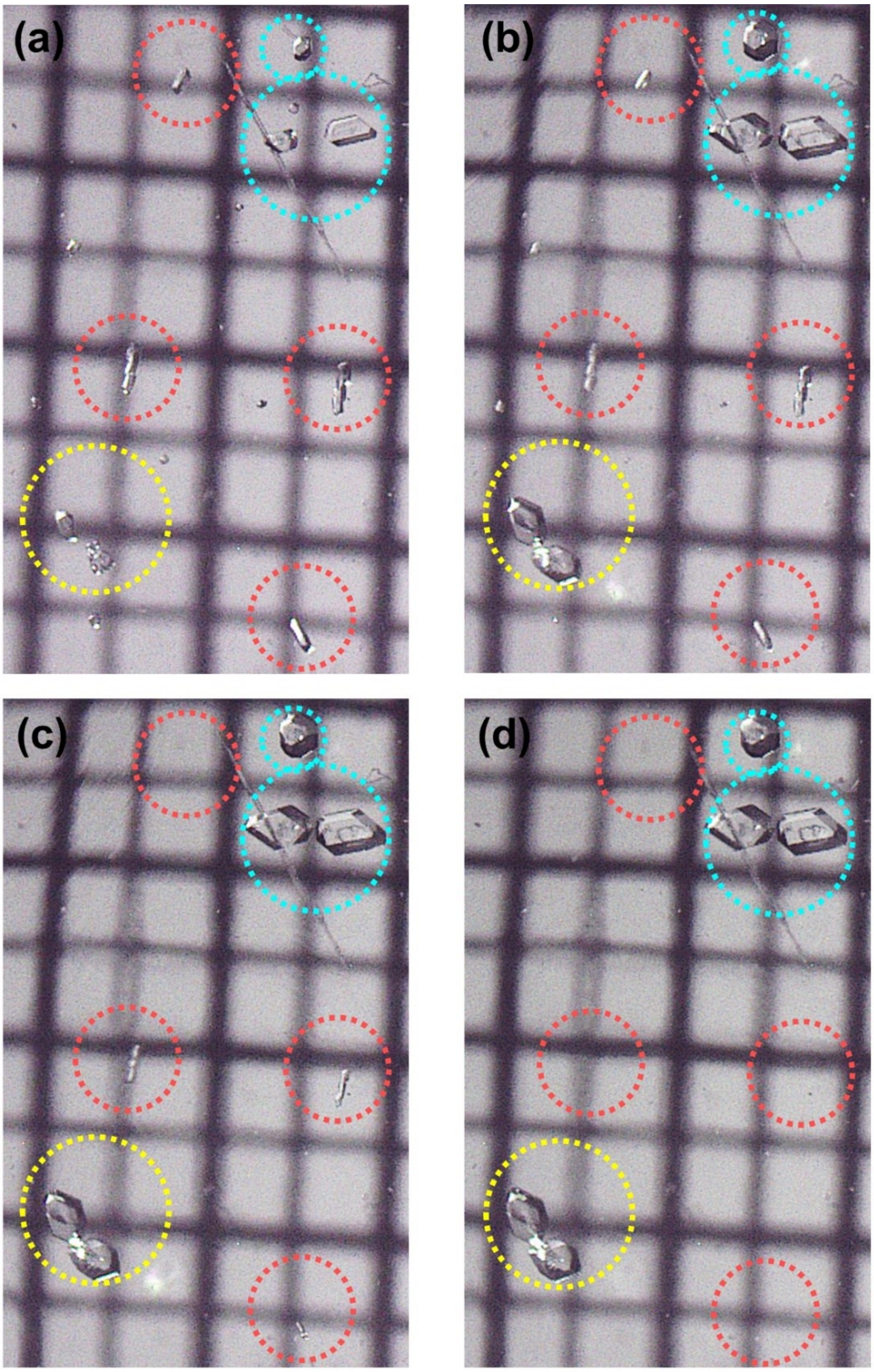

Figure S1 Crystallization and recrystallization processes. Cyan – growth of blocks (**3**), red – disappearance of needles (**1** or **2**), yellow – transformation needle (**1** or **2**) → block (**3**). Letters (a)-(d) indicate time sequence.

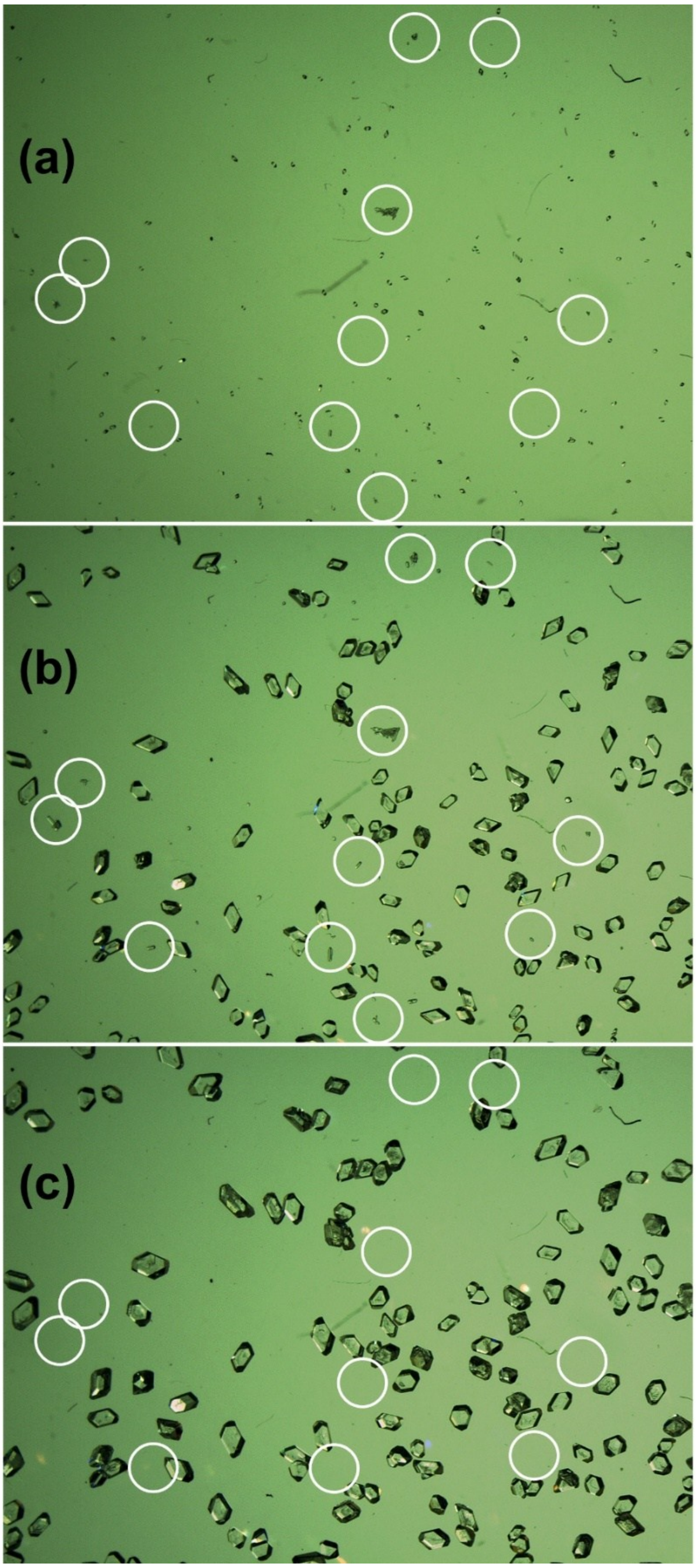

Figure S2 Growth of blocks (**3**) and disappearance of needles (**1** or **2**). Letters (a)-(c) indicate time sequence.

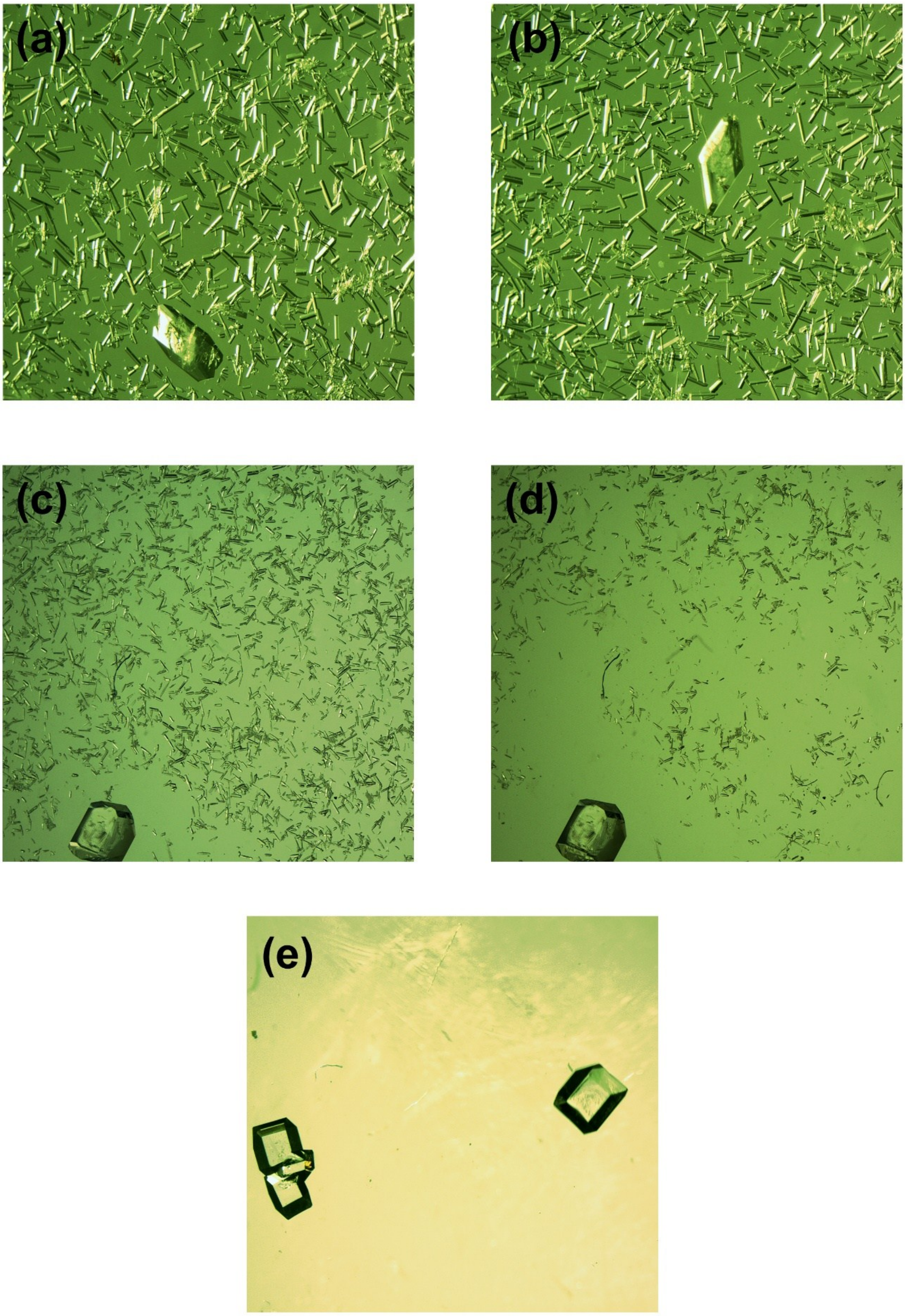

Figure S3 Block (**3**) surrounded by needles (**1** or **2**) (a-d), disapearrance of needles (c-d) and final blocks after recrystalization process (e).

II. Structural description

Details of structural description

Table S1 Crystal data and structure refinement for **1-3** and $(PPh_4)_2[Pt(CN)_4]\cdot H_2O$ (**Pt**).

Identification code	**1**	**2**	**3**	**Pt**
Empirical formula	$C_{60}H_{40}N_{10}P_2Pt$	$C_{62}H_{44}Cl_4N_{10}P_2Pt$	$C_{70}H_{44}Cl_4N_{16}P_2Pt$	$C_{52}H_{42}N_4OP_2Pt$
Formula weight	1158.05	1327.90	1508.04	995.92
Temperature/K	220	120	120	100
Crystal system	triclinic	Triclinic	triclinic	monoclinic
Space group	P-1	P-1	P-1	$P2_1/n$
a/Å	7.4207(12)	11.2950(2)	11.4938(3)	10.4893(2)
b/Å	13.813(2)	11.6539(2)	12.2977(4)	15.9398(4)
c/Å	13.904(2)	12.4440(2)	12.9083(4)	12.9612(3)
α/°	110.437(5)	89.4390(10)	106.1210(10)	90
β/°	102.133(5)	65.2230(10)	101.0370(10)	94.7400(10)
γ/°	92.075(5)	77.9250(10)	105.2820(10)	90
Volume/$Å^3$	1296.2(4)	1448.72(4)	1620.42(9)	2159.67(8)
Z	1	1	1	2
$\rho_{calc}g/cm^3$	1.484	1.522	1.545	1.532
μ/mm^{-1}	2.818	2.711	2.436	3.367
F(000)	578.0	662.0	752.0	996.0
Crystal size/mm^3	0.13 × 0.05 × 0.03	0.32 × 0.08 × 0.05	0.51 × 0.265 × 0.14	0.14 × 0.08 × 0.03
Radiation	MoKα (λ = 0.71073)	MoKα (λ = 0.71073)	MoKα (λ = 0.71073)	MoKα (λ = 0.71073)
2Θ range for data collection/°	5.278 to 50.048	4.784 to 55.756	4.32 to 54.968	4.66 to 50.054
Index ranges	$-8 \le h \le 8$, $-16 \le k \le 16$, $-16 \le l \le 16$	$-14 \le h \le 14$, $-15 \le k \le 15$, $-16 \le l \le 16$	$-14 \le h \le 14$, $-15 \le k \le 15$, $-16 \le l \le 16$	$-12 \le h \le 12$, $-18 \le k \le 18$, $-15 \le l \le 15$
Reflections collected	15299	25042	23148	27343
Independent reflections	4552 [R_{int} = 0.0696, R_{sigma} = 0.0745]	6846 [R_{int} = 0.0472, R_{sigma} = 0.0435]	7390 [R_{int} = 0.0227, R_{sigma} = 0.0235]	3814 [R_{int} = 0.0799, R_{sigma} = 0.0449]
Data/restraints/parameters	4552/0/331	6846/0/358	7390/0/421	3814/0/280
Goodness-of-fit on F^2	1.048	1.021	1.052	1.041
Final R indexes [I>=2σ (I)]	R_1 = 0.0414, wR_2 = 0.0593	R_1 = 0.0291, wR_2 = 0.0609	R_1 = 0.0222, wR_2 = 0.0557	R_1 = 0.0296, wR_2 = 0.0486
Final R indexes [all data]	R_1 = 0.0568, wR_2 = 0.0630	R_1 = 0.0313, wR_2 = 0.0618	R_1 = 0.0222, wR_2 = 0.0557	R_1 = 0.0559, wR_2 = 0.0541
Largest diff. peak/hole / e $Å^{-3}$	1.15/ -0.70	1.48/ -0.95	1.22/ -1.43	1.14/-0.83

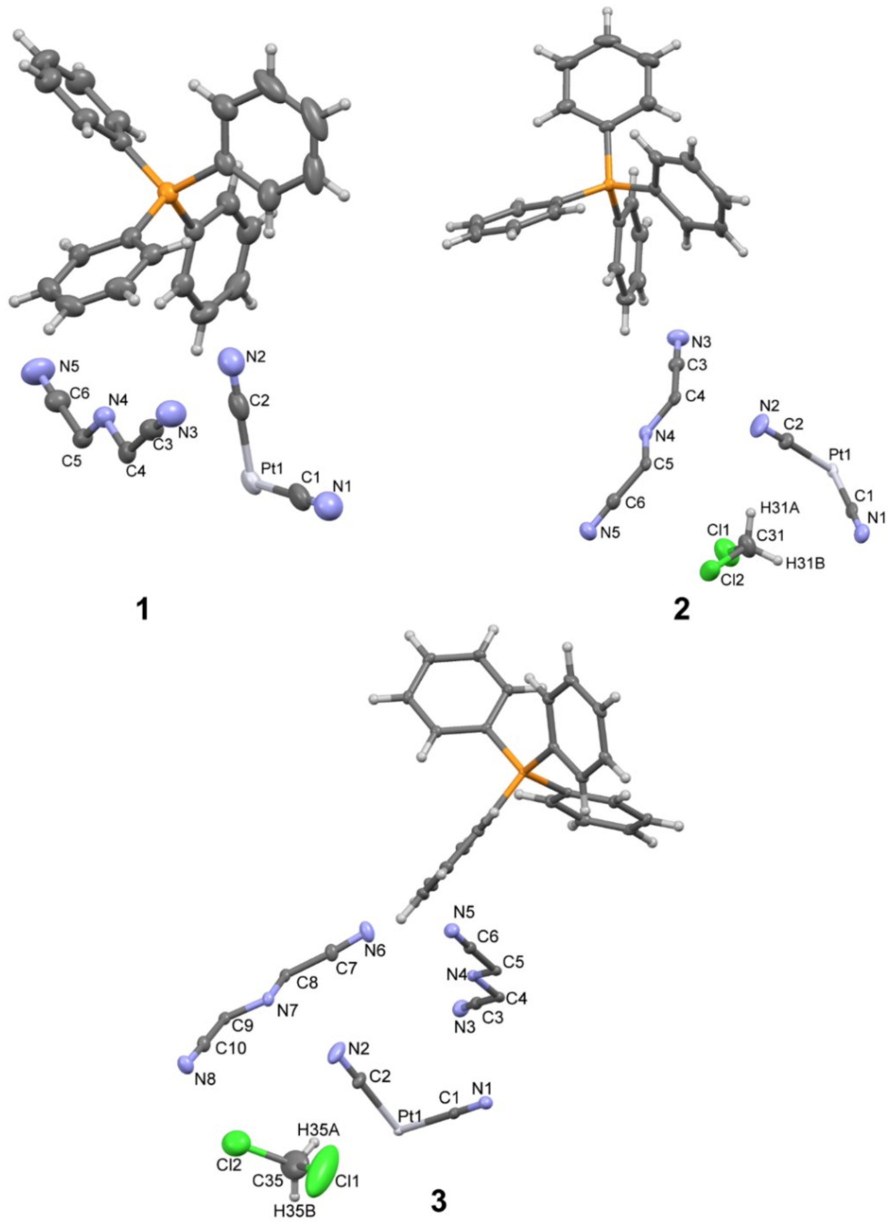

Figure S4 Asymmetric units of **1**-**3**. Colors: Pt – pale grey, P – orange, N – blue, C – dark grey, H – grey. Thermal ellipsoid are drawn at the 50% probability level. The crystal structures of **1** are composed of TCP molecules, $[Pt(CN)_4]^{2-}$ anions and $[PPh_4]^+$ cations (the asymmetric unit contains 1/2 of TCP 1/2 of $[Pt(CN)_4]^{2-}$ and 1 $[PPh_4]^+$ moieties). In contrast to compounds **2** and **3,** structure **1** does not contain solvent molecules. The crystal structures of **2** are composed of TCP molecules, $[Pt(CN)_4]^{2-}$ anions, $[PPh_4]^+$ cations and CH_2Cl_2 molecules (the asymmetric unit contains 1/2 of TCP 1/2 of $[Pt(CN)_4]^{2-}$, 1 $[PPh_4]^+$ and 1 CH_2Cl_2 moieties). The crystal structures of **3** are composed of TCP molecules, $[Pt(CN)_4]^{2-}$ anions, $[PPh_4]^+$ cations and CH_2Cl_2 molecules (the asymmetric unit contains 2 · 1/2 of TCP, 1/2 of $[Pt(CN)_4]^{2-}$, 1 $[PPh_4]^+$ and 1 CH_2Cl_2 moieties).

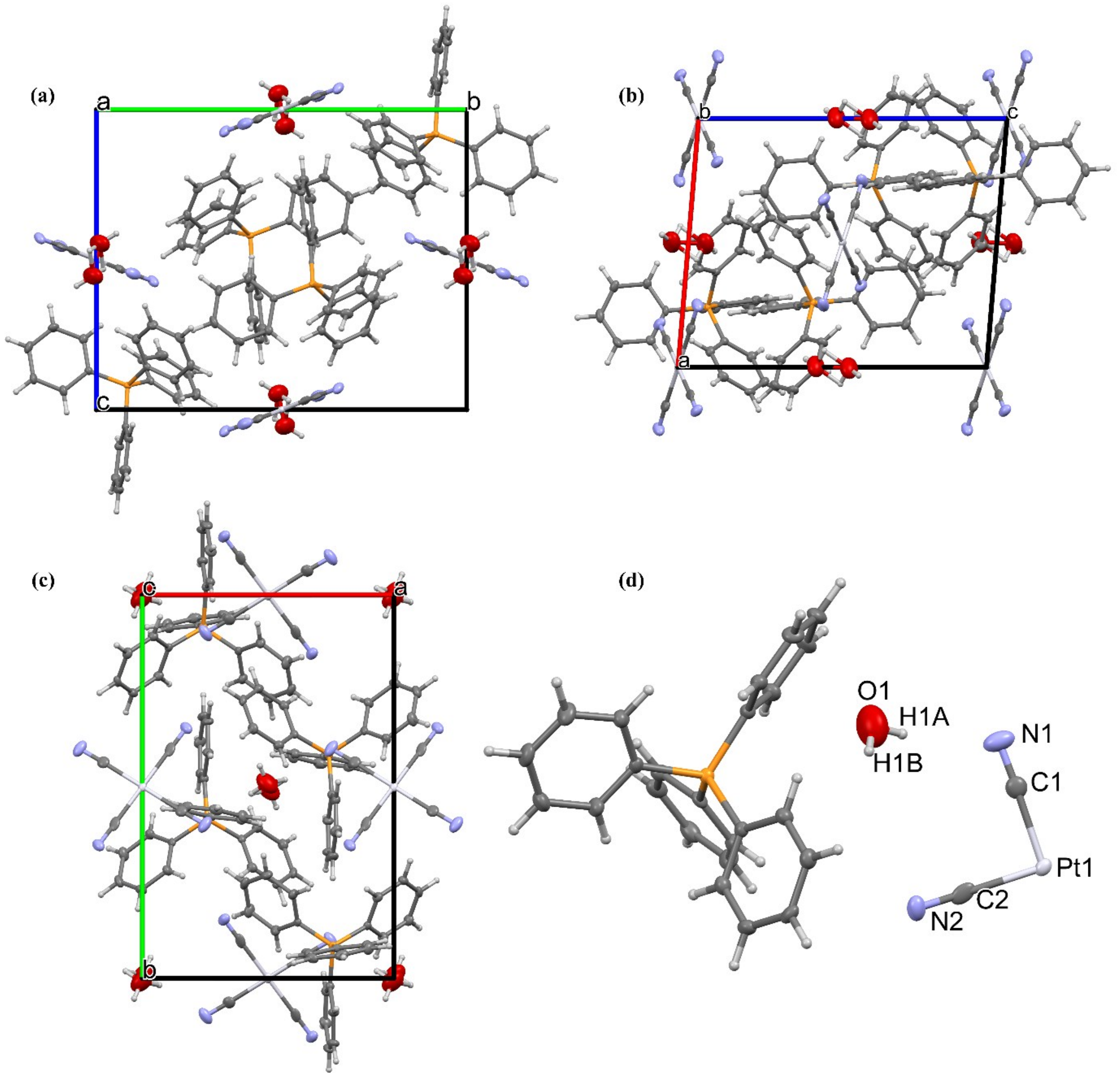

Figure S5 The crystal structure of $(PPh_4)_2[Pt(CN)_4]\cdot H_2O$ (**Pt**): crystal packing along the period *a* (a), *b* (b), *c* (c) and asymmetric unit (d). Colors: Pt – pale grey, P – orange, N – blue, C – dark grey, H – grey. Thermal ellipsoid are drawn at the 50% probability level. The crystal structure of **Pt** is composed of $[Pt(CN)_4]^{2-}$ anions, $[PPh_4]^+$ cations and water molecules (the asymmetric unit contains 1/2 of $[Pt(CN)_4]^{2-}$, 1 $[PPh_4]^+$ and 1 H_2O moieties).

Table S2 List of bonds lengths in **1-3** and in **Pt** crystal structures. The ' sign refers to the atoms reconstructed by appropriate symmetry operations.

Bond	**Length / Å**	**Angle**	**Angle [deg]**
1			
$[Pt(CN)_4]^{2-}$			
Pt1-C1	1.997(5)	C1’-Pt1-C2	89.1(2)
Pt1-C2	1.995(5)	C1’-Pt1-C2’	90.9(2)
C1-N1	1.153(5)	Pt1-C1-N1	178.6(4)
C2-N2	1.153(5)	Pt1-C2-N2	179.3(4)
TCP			
Pyrazine Ring			
C4^{2}-C5	1.398(5)	C4-N4-C5	115.7(3)
C4-N4	1.332(5)	N4-C4-C5	121.9(4)
C5-N4	1.322(5)	N4-C5-C4	122.4(4)
Carbonitrile groups			
C4-C3	1.464(6)	C4-C3-N3	179.3(5)
C5-C6	1.451(6)	C5-C6-N5	177.6(5)
C3-N3	1.140(5)		
C6-N5	1.137(5)		
2			
$[Pt(CN)_4]^{2-}$			
Pt1-C1	1.995(3)	C1’-Pt1-C2	90.6(1)
Pt1-C2	1.989(3)	C1’-Pt1-C2’	89.4(1)
C1-N1	1.151(3)	Pt1-C1-N1	178.5(2)
C2-N2	1.142(4)	Pt1-C2-N2	177.9(3)
TCP			
Pyrazine Ring			
C4-C5	1.403(3)	C4-N4-C5	115.6(2)
C4-N4	1.330(3)	N4-C4-C5	122.5(2)
C5-N4	1.331(3)	N4-C5-C4	121.8(2)
Carbonitrile groups			
C4-C3	1.464(6)	C4-C3-N3	177.6(5)
C5-C6	1.451(6)	C5-C6-N5	179.3(5)
C3-N3	1.153(5)		
C6-N5	1.137(5)		

Bond	**Length / Å**	**Angle**	**Angle [deg]**
3			
$[Pt(CN)_4]^{2-}$			
Pt1-C1	2.005(2)	C1’-Pt1-C2	90.9(1)
Pt1-C2	2.009(2)	C1’-Pt1-C2’	89.1(1)
C1-N1	1.146(3)	Pt1-C1-N1	178.9(2)
C2-N2	1.136(3)	Pt1-C2-N2	178.4(2)
TCP			
Pyrazine ring			
C4-C5	1.411(3)	C4-N4-C5	115.6(2)
C4-N4	1.329(3)	N4-C4-C5	122.3(2)
C5-N4	1.331(3)	N4-C5-C4	122.1(2)
C8-C9	1.406(3)	C8-N7-C9	115.6(2)
C8-N7	1.331(3)	N7-C8-C9	122.1(2)
C9-N7	1.334(3)	N7-C9-C8	122.3(2)
Carbonitrile groups			
C4-C3	1.447(3)	C4-C3-N3	176.5(2)
C5-C6	1.445(3)	C5-C6-N5	176.1(2)
C3-N3	1.144(3)		
C6-N5	1.145(3)		
C8-C7	1.445(3)	C8-C7-N6	175.4(2)
C9-C10	1.450(3)	C9-C10-N8	176.5(2)
C7-N6	1.144(3)		
C10-N8	1.140(3)		
Pt			
$[Pt(CN)_4]^{2-}$			
Pt1-C1	1.985(5)	C1’-Pt1-C2	89.5(2)
Pt1-C2	1.993(5)	C1’-Pt1-C2’	90.5(2)
C1-N1	1.165(6)	Pt1-C1-N1	177.7(5)
C2-N2	1.152(6)	Pt1-C2-N2	178.8(4)

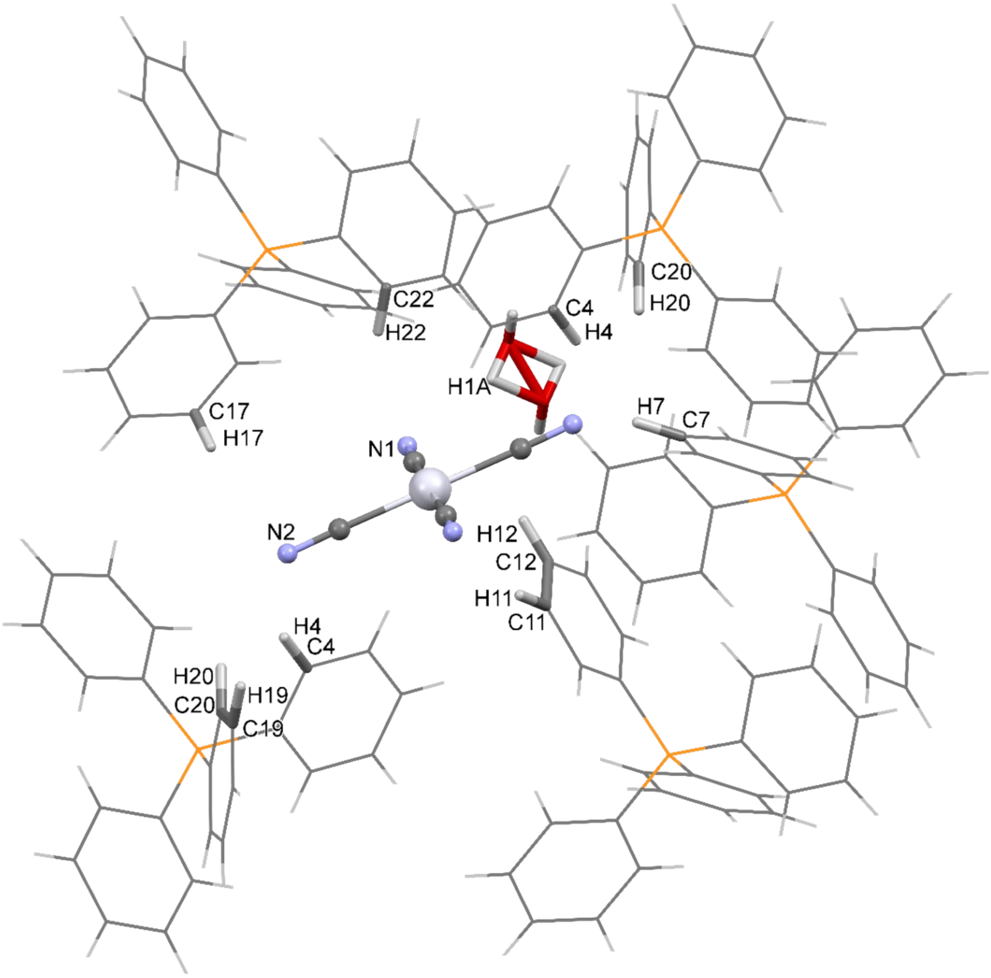

Figure S6 The crystal structure of $(PPh_4)_2[Pt(CN)_4]\cdot H_2O$ (**Pt**): the molecular surrounding of $[Pt(CN)_4]^{2-}$ involving protons of phenyl rings and water molecule. Short contacts of CN-ligands and metal center with hydrogen atoms are listed in **Table S3**.

Table S3 Short contacts with hydrogen atoms in **Pt**. The uncertainties of measured donor – H, acceptor – H, distances and angles cannot be estimated due to positions of hydrogen atoms within structures, which were placed in idealized positions and refined using riding coordinate model.

Atoms names / A···H – D	**Angle A···H – D [deg]**	**Distance H···A [Å]**
N1···H1A – O1	154.3	2.318
N1···H22 – C22	157.4	2.640
N1···H19 – C19	127.4	2.823
N1···H12 – C12	153.9	2.785
N1···H18 – C18	118.4	3.042
N2···H17 – C17	145.9	2.657
N2···H7 – C7	132.1	2.519
N2···H4 – C4	150.2	2.392
N2···H20 – C20	147.8	2.679
Pt···H11 – C11	145.6	3.111

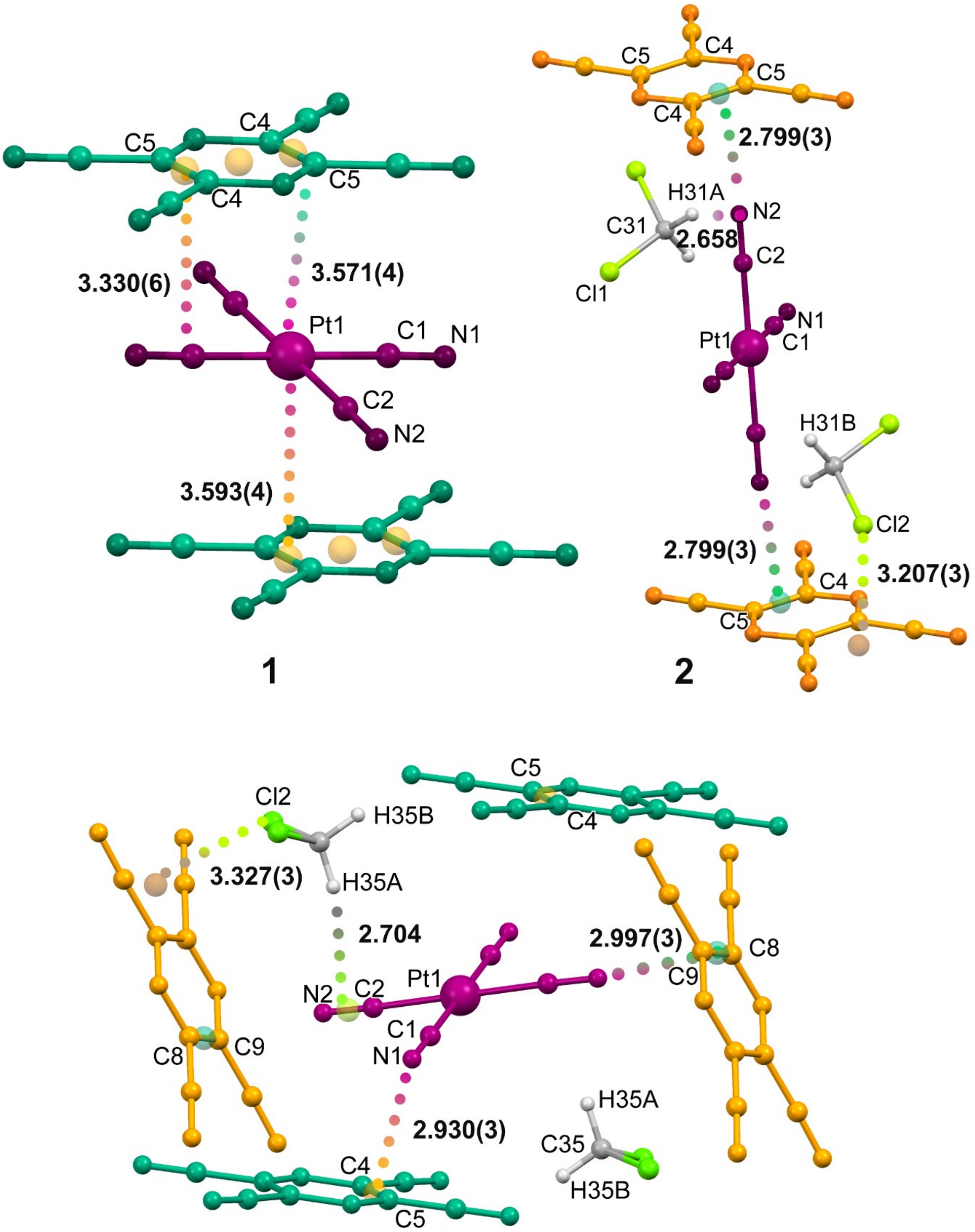

1

2

3

Figure S7 Close contacts in synthons based on TCP, anion (**1**, **2**, **3**) and CH_2Cl_2 (**2** and **3**) molecules. Anion-π contacts $[Pt(CN)_4]^{2-}\cdots$TCP involve the respective regions of negative and positive electrostatic potentials. The stabilizing effect of solvent molecule is also highlighted. The selected interaction contacts are marked with dotted lines and the related distances are indicated.

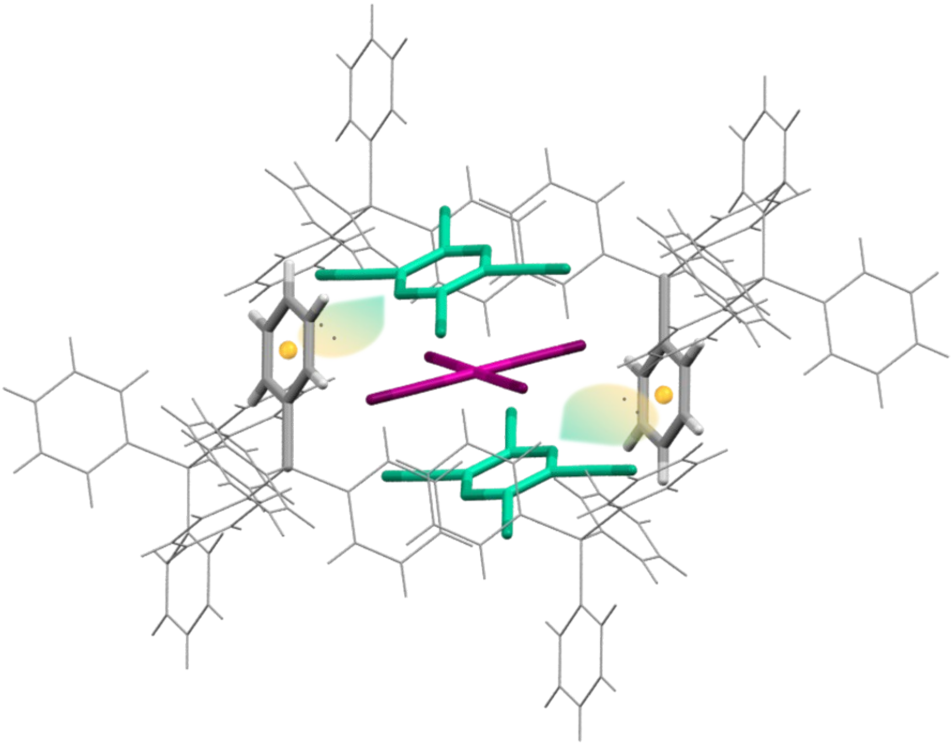

Figure S8 Lone pair - π interaction contacts between nitrogen (TCP) and phenyl ring of PPh_4^+ cation in **1**. The distance from nitrogen atom to ring's centroid $N_{ring,TCP}$...$centr_{Ph}$ is *ca.* 3.6 Å, while the distance from nitrogen atom to the closest carbon atom $N_{ring,TCP}$...C10 is *ca.* 3.2 Å.

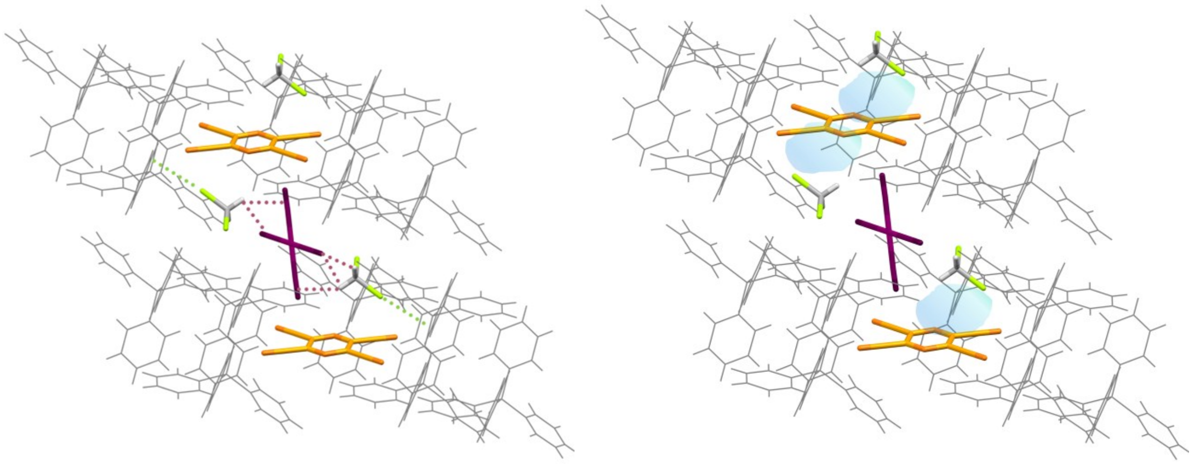

Figure S9 Cation···solvent···$[Pt(CN)_4]^{2-}$ interactions (the shortest distance –CN···H: *ca.* 2.6 Å) and solvent···TCP interaction (H···$TCP_{centroid}$: 3.6 *ca.* Å, –CN···Cl *ca.* 3.5 Å) in **2**.

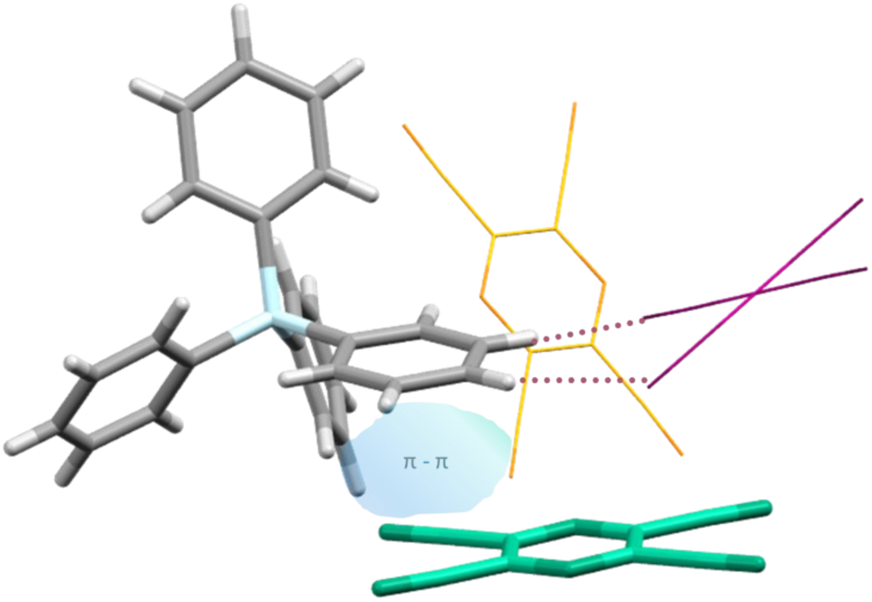

Figure S10 π-π interaction part (dist. *ca.* 3.3 Å) and short contact H···NC in **3**.

The different arrangement of TCP with respect to the anionic metal complex in **2** and **3** *vs*. **1** is the consequence of the exposition of its molecular surface to the surrounding environment, which consists mostly of nearby PPh_4^+ cations. The structural evolution (**1**,**2**→**3**) involves, for example, a decrease of the $_{pyz}N \cdots P_{cation}$ distance from 5.8 Å in **1** to 4.6 Å in **2** and **3** (**Figure S11** and **Figure S12**) This strengthens the attraction between the lone-pair of pyrazine nitrogen atoms with the positive potential around the "pocket" of the nearby PPh_4^+ cation and interactions of TCP's $N_{nitrile}$ atoms with H-C_{Phenyl} groups of PPh_4^+. Furthermore, in **3** the "second" TCP molecule (green along all related Figures) forms offset sandwich-like motifs with two neighboring phenyl rings from adjacent PPh_4^+ molecules. Distances H-A (hydrogen-acceptor) and angles D-H-A (donor-hydrogen-acceptor), where acceptor is -CN group, are listed in **Table S4**.

Table S4 Short contacts with hydrogen atoms in **1-3**. The uncertainties of measured donor – H, acceptor – H, distances and angles cannot be estimated due to positions of hydrogen atoms within structures, which were placed in idealized positions and refined using riding coordinate model.

	Atoms names /D-H···A	**Distance H···A [Å]**	**Angle D-H···A [deg]**
1	**TCP**		
	C22-H22···N3	2.618	139.10
	C27-H27···N5	2.573	149.39
	$[Pt(CN)_4]^{2-}$		
	C10-H10···N2	2.743	123.59
	C17-H17···N1	2.640	155.16
	C29-H29···N1	2.710	164.95
2	**TCP**		
	C24-H24···N3	2.806	126.24
	C26-H26···N3	2.724	108.48
	C31-H31A···C5	3.623	111.40
	$[Pt(CN)_4]^{2-}$		
	C10-H10···C1	2.898	128.59
	C16-H16···N1	2.588	139.02
	C28-H28···N1	2.489	153.57
	C31-H31A···N2	2.658	153.18
	C31-H31B···N1	2.585	136.38
3	**TCP parallel**		
	C30-H30···N5	2.521	159.26
	C35-H35B···N3	2.631	146.02
	TCP perpendicular		
	C22-H22···N7	2.698	163.01
	$[Pt(CN)_4]^{2-}$		
	C20-H20···N1	2.548	141.31
	C35-H35A···C2	2.714	174.32

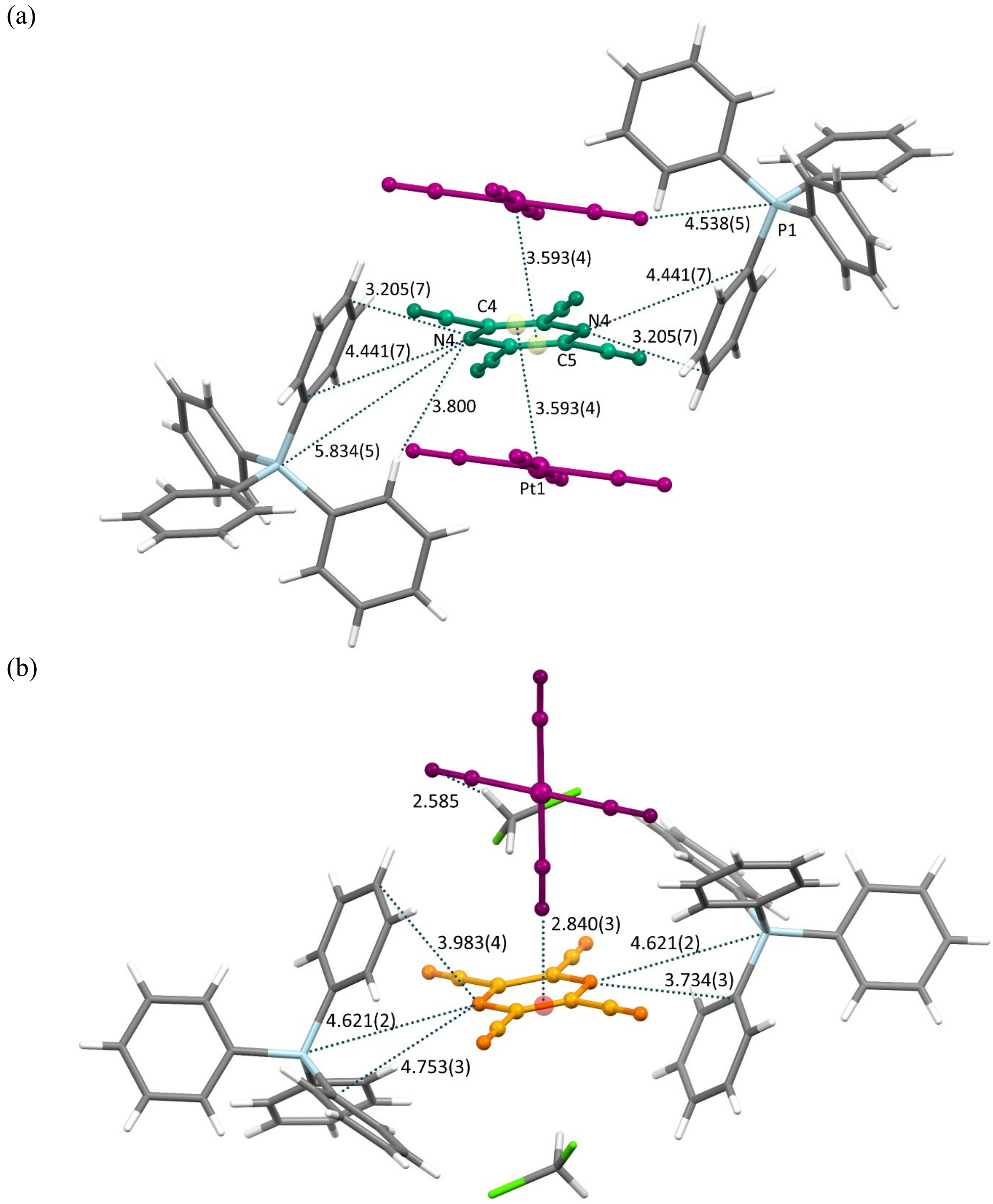

Figure S11 The comparison of the contacts between nitrogen lone pair of pyrazine of TCP and positive potential pocket of PPh_4^+ in **1** (a) and **2** (b).

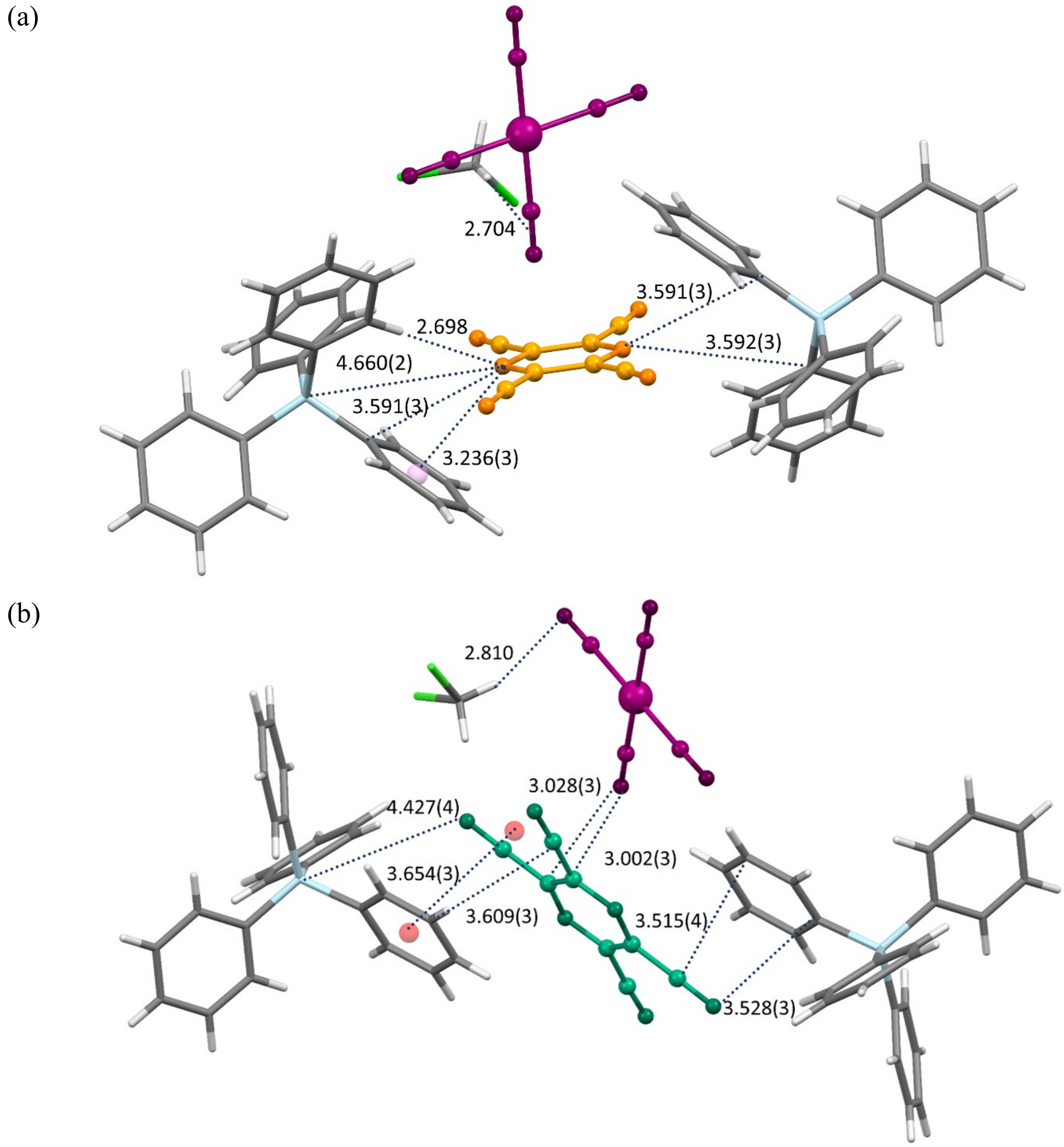

Figure S12 The contacts between the positive potential pocket of PPh_4^+ and nitrogen lone pairs of TCP in **3**: pyrazine nitrogen (a) and nitrile nitrogen (b). Compare the position of CH_2Cl_2 molecule with the relevant arrangement in **2**, **Figure S11b**.

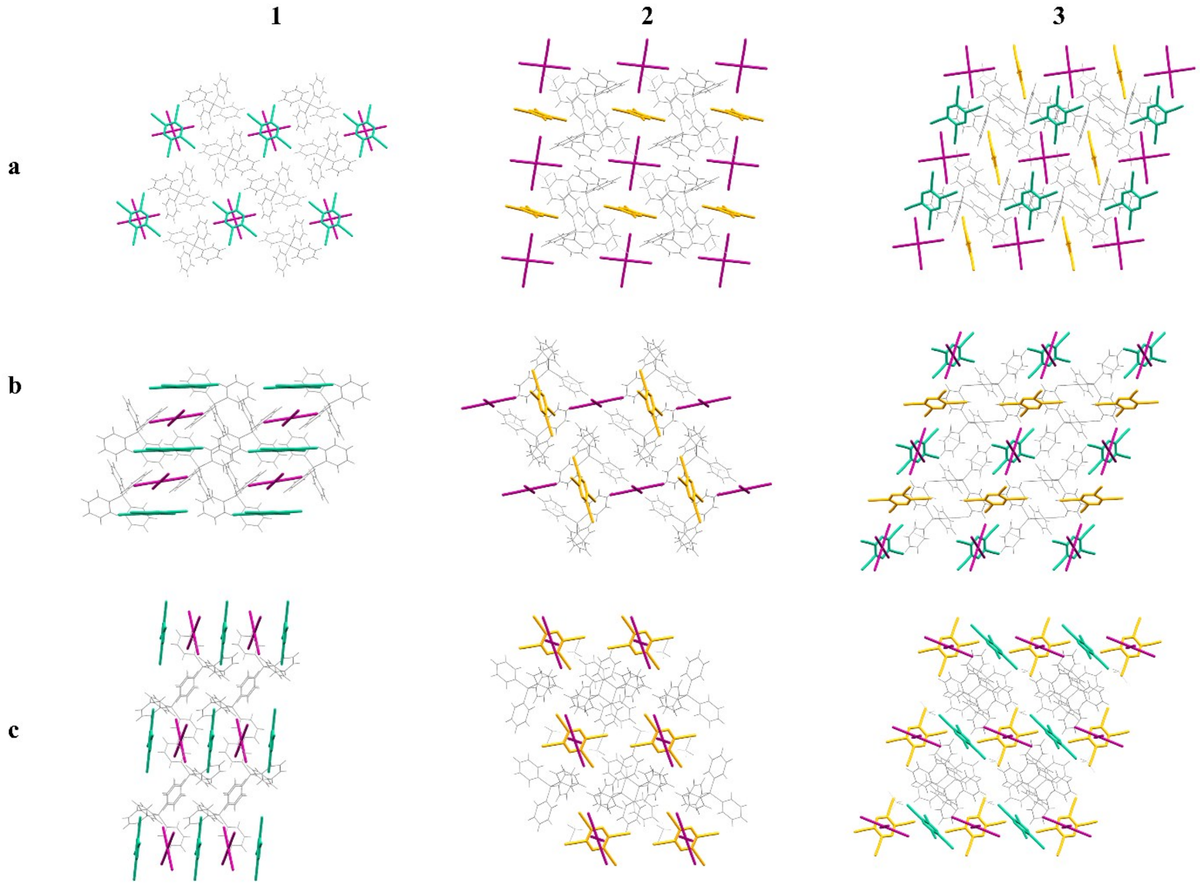

Figure S13 Packing of **1**-**3** (columns) along the crystallographic axes *a*, *b* and *c* (rows). Colors: pink – $[Pt(CN)_4]^{2-}$, green – parallel TCP, yellow – perpendicular TCP, grey – PPh_4^+, pale grey – CH_2Cl_2.

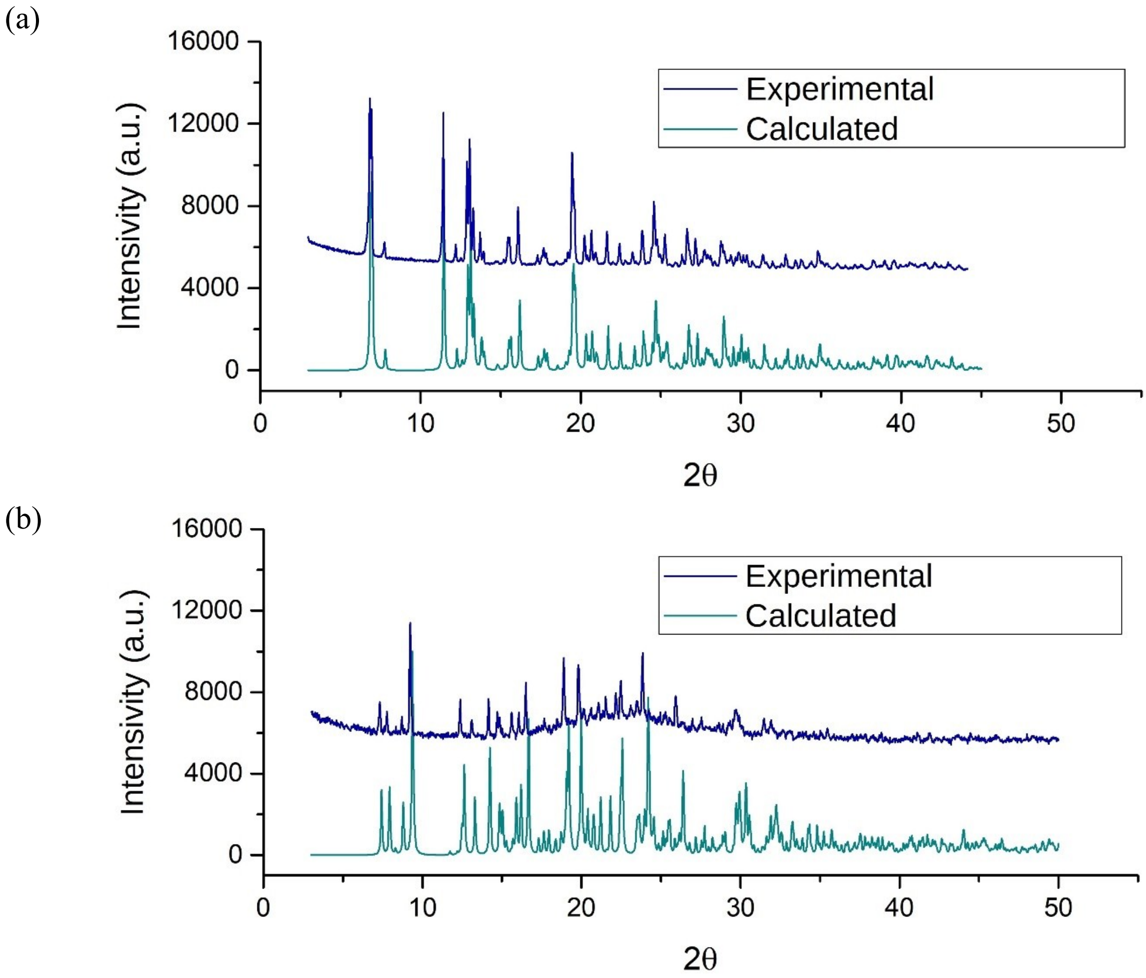

Figure S14 Powder X-ray diffraction patterns of **1** (a) and **3** (b) in the 4-50° range of 2Θ angle: experimental (navy blue) and calculated from single crystal X-ray model (turquoise). Shift of PXRD peaks in relation to the calculated from XRD is related to standard temperature effect. XRD (120 K), PXRD (RT).

III. Spectroscopic characterization

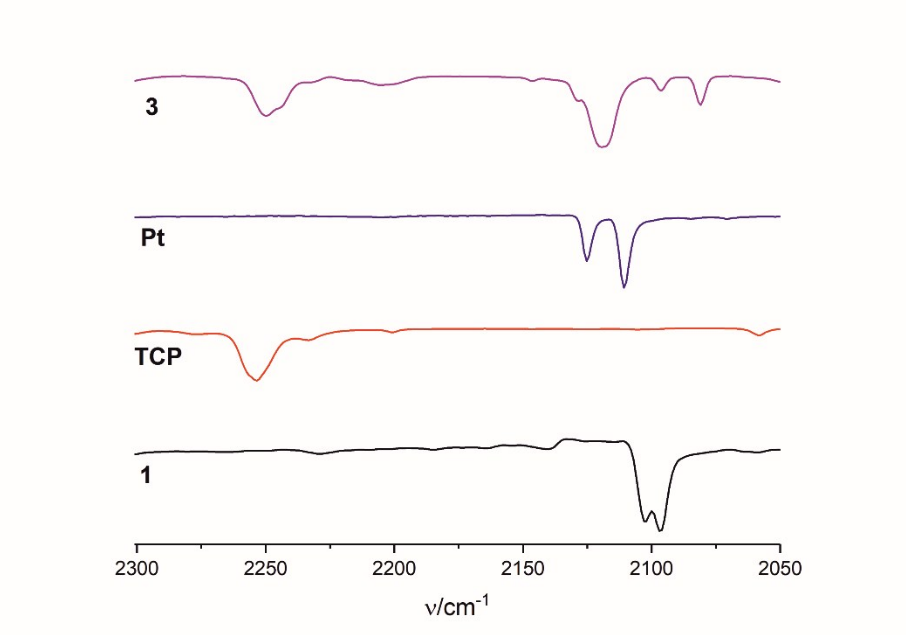

Figure S15 Infrared spectra (CN range) of **1** (black) and **3** (magenta) in comparison to TCP (red) and $(PPh_4)_2[Pt(CN)_4]\cdot H_2O$ (**Pt**) (blue).

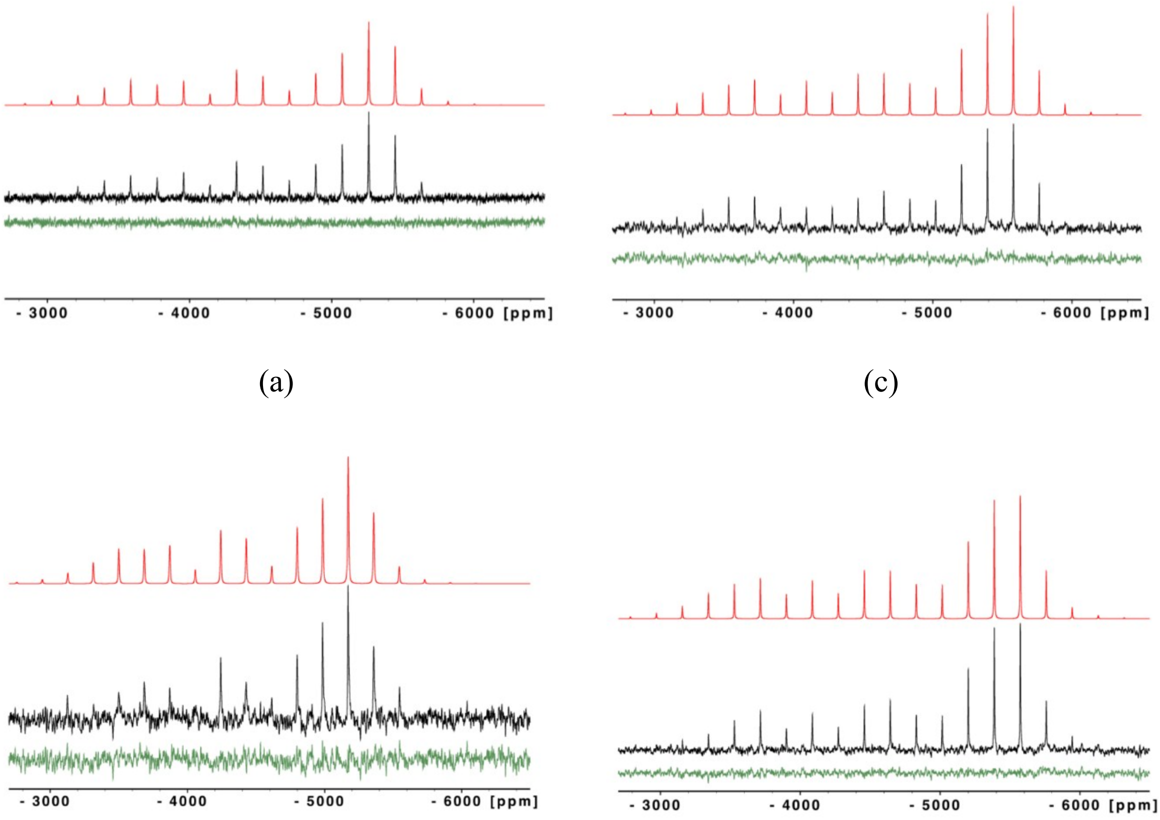

(a) (c)

(b) (d)

Figure S16 The fitting of the solid-state ^{195}Pt NMR spectrum for **1** (a), **Pt-HAT(CN)$_6$** (b), **3** (c) and $(PPh_4)_2[Pt(CN)_4]\cdot H_2O$ (**Pt**) (d): fitted (red), experimental (black) and difference (green).

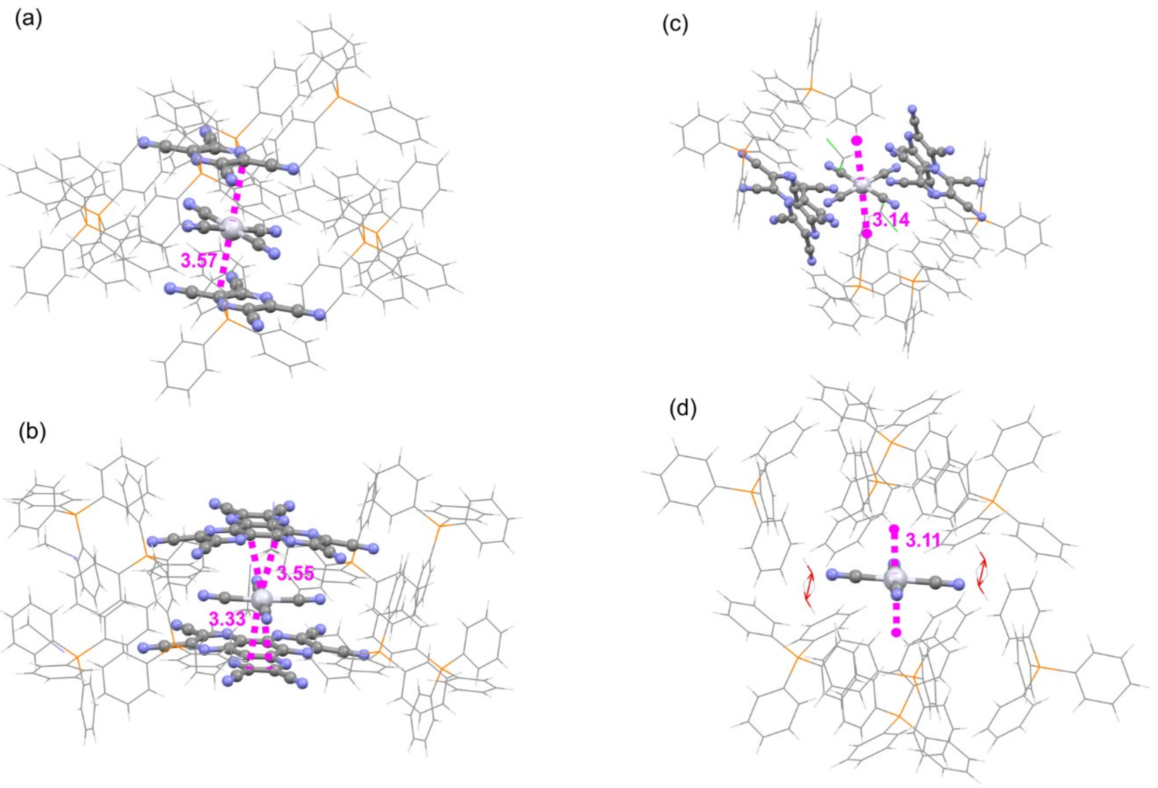

Figure S17 The comparison of the axial contacts formed by Pt^{II} centers in $[Pt(CN)_4]^{2-}$ in the crystal structure of **1** (a), **Pt-HAT(CN)$_6$** (b), **3** (c) and $(PPh_4)_2[Pt(CN)_4]\cdot H_2O$, **Pt**, (d). **1** and **Pt-HAT(CN)$_6$** reveal exclusively the direct contact with the extended flat positive potential of the π-acid, $Pt\cdots C_{ring}$ of 3.3 to 3.6 Å, whereas **3** and **Pt** show only the point head-on $Pt\cdots H_{phenyl}$ contacts of 3.1 Å. The equatorial in-plane contacts between nitrogen atoms of CN^- ligands and phenyl or H_2O (**Pt**) are the examples of very weak hydrogen bonds of the minor importance to the electronic cloud on Pt center. See also the ETS-NOCV analysis presented in **Figure S21** and **Figure S28** for **1**, **3** and **Pt**, and for **Pt-HAT(CN)$_6$**.[2b] Note that for **1** and **Pt-HAT(CN)$_6$** energetically effective, direct mixing of molecular states of TCP and $HAT(CN)_6$, respectively, with Pt *d* orbitals is visible with a gain in electron density between the π-acceptor and the metal center.

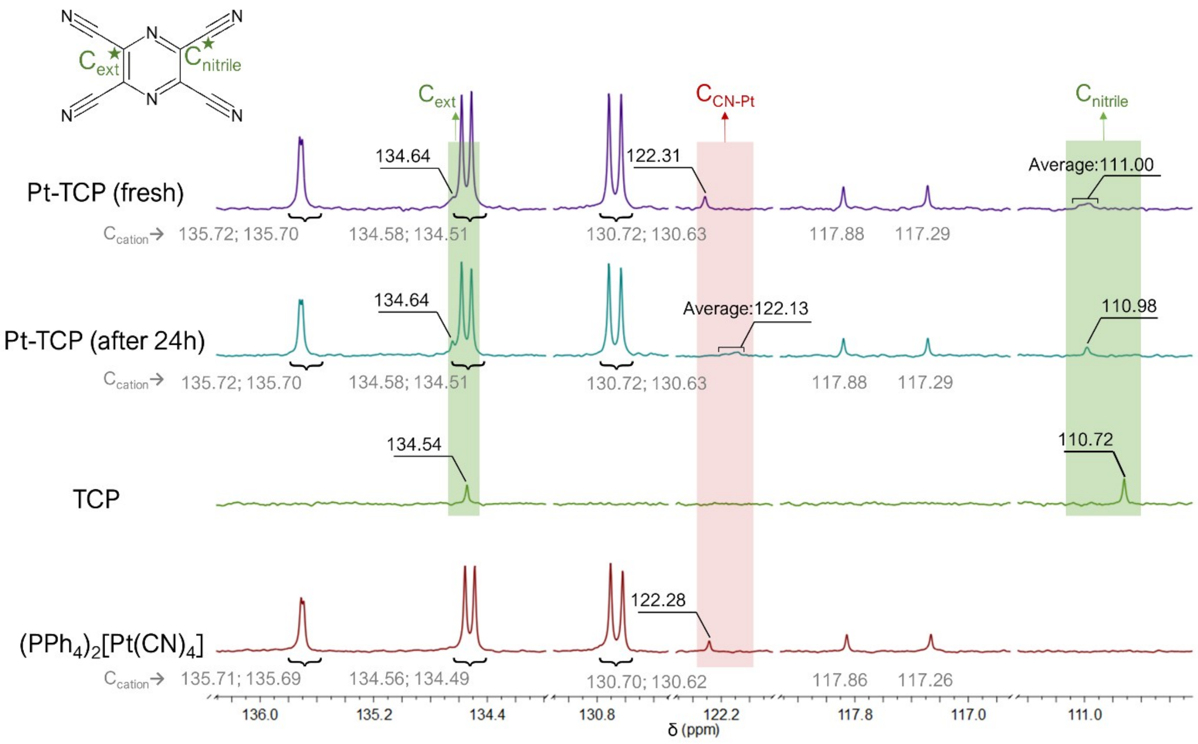

Figure S18 ^{13}C NMR spectra of substrates (red - TCP, green - $(PPh_4)_2[Pt(CN)_4]$) and adduct (violet - fresh solution, turquoise - after 24 hours) in CH_2Cl_2. Concentration: TCP, $(PPh_4)_2[Pt(CN)_4]$ = 0.009 mol/dm^3, adduct = 0.0045 mol/dm^3. The shaded bars indicate the regions of interest in which the chemical shifts change. In the case of $C_{CN\text{-}Pt}$ / $C_{nitrile}$, broadening / sharpening of signal is observed with time, thus only average δ value is presented.

Table S5 Observed ^{13}C NMR chemical shifts of CN^- ligand in $[Pt(CN)_4]^{2-}$ ($C_{CN\text{-}Pt}$) and of nitrile substituents and C4° pyrazine in TCP ($C_{nitrile}$ and C_{ext}, respectively). Compare with **Figure S18**.

	δ(ppm)			
	Pt-TCP (fresh)	Pt-TCP (after 24h)	TCP	$(PPh_4)_2[Pt(CN)_4]$
$C_{CN\text{-}Pt}$	122.31	122.17/122.08	-	122.28
$C_{nitrile}$	111.03/110.98	110.98	110.72	-
C_{ext}	134.64	134.64	134.54	-

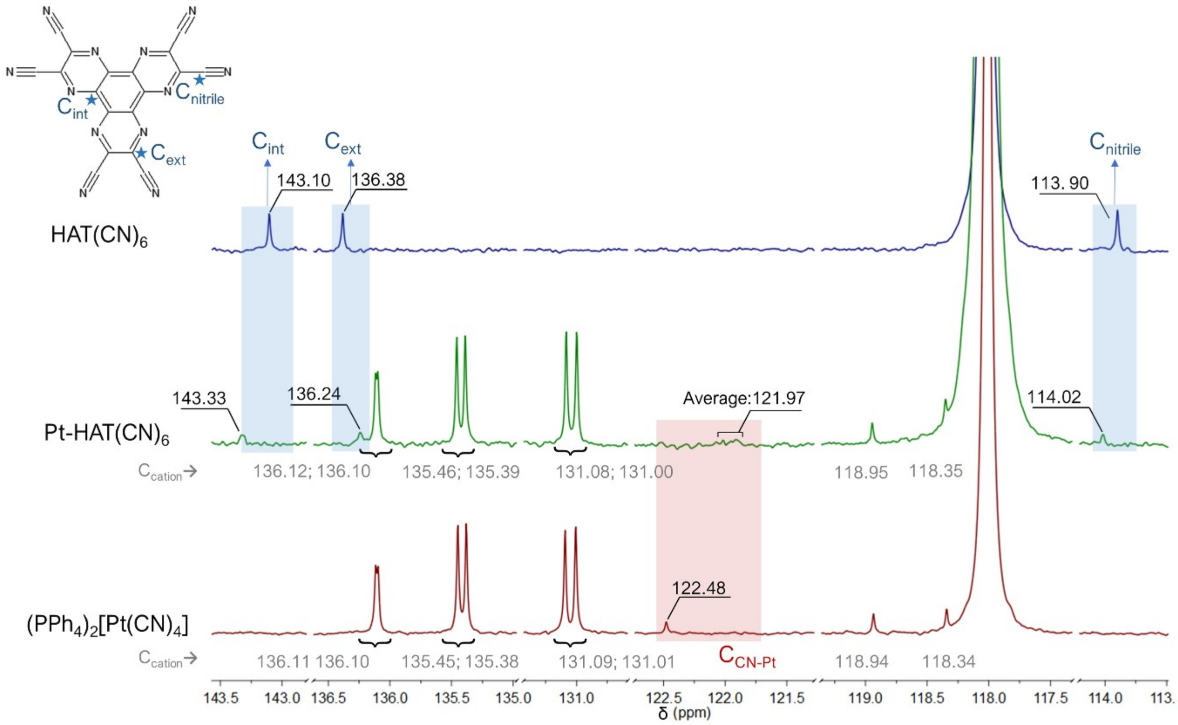

Figure S19 ^{13}C NMR spectra of HAT(CN)$_6$ (blue), (PPh$_4$)$_2$[Pt(CN)$_4$] (red) and adduct (green) in MeCN (acetonitrile). Concentration: HAT(CN)$_6$, (PPh$_4$)$_2$[Pt(CN)$_4$] = 0.009 mol/dm^3, adduct = 0.0045 mol/dm^3. The shaded bars indicate the regions of interest in which the chemical shifts change. In the case of C$_{CN\text{-}Pt}$ broadening of signal is observed with time, thus only average δ value is presented.

Table S6 Observed ^{13}C NMR chemical shifts of CN$^-$ ligand in [Pt(CN)$_4$]$^{2-}$ (C$_{CN\text{-}Pt}$) and of nitrile substituents and C4° pyrazine and benzene rings in HAT(CN)$_6$ (C$_{nitrile}$, C$_{ext}$, and C$_{int}$, respectively). Compare with **Figure S19**.

	δ(ppm)		
	Pt-HAT(CN)$_6$	HAT(CN)$_6$	(PPh$_4$)$_2$[Pt(CN)$_4$]
C$_{CN\text{-}Pt}$	121.91/122.02	-	122.48
C$_{nitrile}$	114.02	113.90	-
C$_{ext}$	136.24	136.38	-
C$_{int}$	143.33	143.10	-

IV. Computational part

Computational detail

All calculations were performed using density functional theory (DFT) methods with the Vienna Ab-Initio Simulation Package (VASP)[1], for models of periodic networks, or the Gaussian 09 (G09)[2] and the Amsterdam Density Functional 2016 (ADF2016)[3,4] programs, for models of molecular clusters. The computational analysis protocol that was adopted follows in general that which was established for related systems in References 5, 6, and 7.

Periodic network modelling, based generally on the experimental lattice constants and symmetry elements, employed the PBE[8] exchange-correlation functional coupled with a Hubbard correction potential[9] with U-J = 2 eV and the Grimme post-SCF D3 dispersion correction[10] (PBE+D3+U). The hybrid HSE06 functional[11] was additionally used to compute the electronic densities of states. The plane-wave basis set cutoff was set to 500 eV; the Pt (6s/5d), Cl (3s/3p), N and C (2s/2p), and H (1s) valence electrons were treated explicitly and used in conjunction with PAW[12] potentials that were supplied with the standard VASP package - version 5.2. Calculations were performed on structures **1-3**, $(PPh_4)_2[Pt(CN)_4]\cdot H_2O$ salt, and, for comparison purposes, on the $[PtCl_4]^{2-}$/TCP system reported in Reference 13, and on a

---

[1] Kresse, G.; Furthmüller, J., Efficiency of ab-initio total energy calculations for metals and semiconductors using a plane-wave basis set. *Comput. Mater. Sci.* **1996**, *6* (1), 15-50.

[2] Gaussian 09, R. D., M. J. Frisch, G. W. Trucks, H. B. Schlegel, G. E. Scuseria, M. A. Robb, J. R. Cheeseman, G. Scalmani, V. Barone, B. Mennucci, G. A. Petersson, H. Nakatsuji, M. Caricato, X. Li, H. P. Hratchian, A. F. Izmaylov, J. Bloino, G. Zheng, J. L. Sonnenberg, M. Hada, M. Ehara, K. Toyota, R. Fukuda, J. Hasegawa, M. Ishida, T. Nakajima, Y. Honda, O. Kitao, H. Nakai, T. Vreven, J. A. Montgomery, Jr., J. E. Peralta, F. Ogliaro, M. Bearpark, J. J. Heyd, E. Brothers, K. N. Kudin, V. N. Staroverov, R. Kobayashi, J. Normand, K. Raghavachari, A. Rendell, J. C. Burant, S. S. Iyengar, J. Tomasi, M. Cossi, N. Rega, J. M. Millam, M. Klene, J. E. Knox, J. B. Cross, V. Bakken, C. Adamo, J. Jaramillo, R. Gomperts, R. E. Stratmann, O. Yazyev, A. J. Austin, R. Cammi, C. Pomelli, J. W. Ochterski, R. L. Martin, K. Morokuma, V. G. Zakrzewski, G. A. Voth, P. Salvador, J. J. Dannenberg, S. Dapprich, A. D. Daniels, Ö. Farkas, J. B. Foresman, J. V. Ortiz, J. Cioslowski, D. J. Fox, Gaussian 09, Revision D.01; Gaussian, Inc.: Wallingford CT, 2009.

[3] ADF2016, S., Theoretical Chemistry, Vrije Universiteit, Amsterdam, The Netherlands, http://www.scm.com.

[4] te Velde, G.; Bickelhaupt, F. M.; Baerends, E. J.; Fonseca Guerra, C.; van Gisbergen, S. J. A.; Snijders, J. G.; Ziegler, T., Chemistry with ADF. *J. Comput. Chem.* **2001**, *22* (9), 931-967.

[5] Kobylarczyk, J.; Pinkowicz, D.; Srebro-Hooper, M.; Hooper, J.; Podgajny, R., Anion-π recognition between $[M(CN)_6]^{3-}$ complexes and $HAT(CN)_6$: structural matching and electronic charge density modification. *Dalton, Trans.* **2017**, *46* (11), 3482-3491.

[6] Kuzniak, E.; Pinkowicz, D.; Hooper, J.; Srebro-Hooper, M.; Hetmańczyk, Ł.; Podgajny, R., Molecular deformation, charge flow, and sponge-like behavior in anion-π $\{[M(CN)_4]^{2-};[HAT(CN)_6]\}_\infty$ (M = Ni, Pd, Pt) supramolecular stacks. *Chem. Eur. J.* **2018**, *24* (61), 16302-16314.

[7] Kobylarczyk, J.; Pinkowicz, D.; Srebro-Hooper, M.; Hooper, J.; Podgajny R. Anion-π Architectures of $HAT(CN)_6$ and 5*d* Polycyanidometalates: $[W(CN)_8]^{3-}$, $[Re(CN)_7]^{3-}$, and $[Pt(CN)_6]^{2-}$. *Cryst. Growth Des.* **2019**, *19* (2), 1215-1225.

[8] Perdew, J. P.; Burke, K.; Ernzerhof, M., Generalized Gradient Approximation Made Simple. *Phys. Rev. Lett.* **1996**, *77* (18), 3865-3868.

[9] Liechtenstein, A. I.; Anisimov, V. I.; Zaanen, J., Density-functional theory and strong interactions: Orbital ordering in Mott-Hubbard insulators. *Phys. Rev. B* **1995**, *52* (8), R5467-R5470.

[10] Grimme, S.; Antony, J.; Ehrlich, S.; Krieg, H., A consistent and accurate ab initio parametrization of density functional dispersion correction (DFT-D) for the 94 elements H-Pu. *J. Chem. Phys.* **2010**, *132* (15), 154104.

[11] Krukau, A. V.; Vydrov, O. A.; Izmaylov, A. F.; Scuseria, G. E., Influence of the exchange screening parameter on the performance of screened hybrid functionals. *J. Chem. Phys.*, **2016**, *125* (22), 224106.

[12] Blöchl, P. E., Projector augmented-wave method. *Phys. Rev. B* **1994**, *50* (24), 17953-17979.

[13] Rosokha, S. V.; Kumar, A., Anion-π interaction in metal-organic networks formed by metal halides and tetracyanopyrazine. *J. Mol. Struc.* **2017**, *1138*, 129-135.

hypothetical $[Pt(CN)_4]^{2-}$-based analogue of this $[PtCl_4]^{2-}$/TCP system (labelled, respectively, as **R** and $\mathbf{R}^{[Pt(CN)4]2-}$ in the following).

The NCIPLOT program[14] was used, as described in the text, to visualize the non-covalent interaction(s) around TCP in **1** and **2**. (**3** is not shown, but the anion-π interactions in **3** are similar to **2**). The reduced density gradient (RDG) isosurface plots (NCI plots) presented in the text are colored by the "sign(λ_2)·ρ" value (λ_2 is the second eigenvalue of the electron-density Hessian matrix), which, as described in the literature,[15] is used to distinguish different types of non-covalent interactions from each other (and sometimes used to assess their stabilities). The critic2[16] and VESTA[17] programs were used to generate the RDG plots.

Modelling of molecular clusters, as extracted from the optimized periodic network coordinates of the systems listed above, involved (*i*) binding energy calculations for a set of two-molecule clusters that were performed with G09 employing the PBE+D3 density functional, the TZVP basis set with the corresponding 60-electron relativistic effective core potential for the Pt atoms,[18,19] and the dichloromethane continuum solvent model PCM,[20] and (*ii*) extended transition state natural orbitals for chemical valence (ETS-NOCV)[21,22] charge and interaction-energy decomposition analysis for a selected clusters (cation-cation, (metal complex)-TCP, (metal complex)-cation) that were carried out with ADF2016 using PBE+D3 along with an (all-electron) triple-ζ Slater-type basis set with two sets of polarization functions (TZ2P) from the ADF basis-set library and the Zeroth-Order Regular Approximation (ZORA) to incorporate scalar relativistic effects.[23,24] Additionally, for a set of freely optimized $[Pt(CN)_4]^{2-}$/TCP clusters and their pristine components, $[Pt(CN)_4]^{2-}$ and TCP, ($[Pt(CN)_4]^{2-}$:TCP = 1:1, BP-D3/SVP[13,25,26,27] calculations with solvent effects (dichloromethane) included via the

---

[14] Contreras-García J.; Johnson E. R.; Keinan, S.; Chaudret, R., Piquemal, J.-P.; Beratan, D. N.; Yang, W., NCIPLOT: a program for plotting non-covalent interaction regions. *J. Chem. Theory Comput.* **2011**, *7* (3), 625-632.

[15] Johnson, E. R.; Keinan, S.; Mori-Sánchez, P.; Contreras-García, J.; Cohen, A. J.; Yang, W., Revealing Noncovalent Interactions. *J. Am. Chem. Soc.* **2010**, *132* (18), 6498-6506.

[16] Otero-de-la-Roza, A.; Johnson, E. R.; Luaña, V., Critic2: A program for real-space analysis of quantum chemical interactions in solids. *Comp. Phys. Comm.* **2014**, *185* (3), 1007-1018.

[17] Momma, K.; Isumi, F., VESTA 3 for three-dimensional visualization of crystal, volumetric and morphology data. *J. Appl. Cryst.* **2011**, *44* (6), 1272-1276.

[18] Weigend, F.; Ahlrichs, R., Balanced basis sets of split valence, triple zeta valence and quadruple zeta valence quality for H to Rn: Design and assessment of accuracy. *Phys. Chem. Chem. Phys.* **2005**, *7* (18), 3297-3305.

[19] Andrae, D.; Häußermann, U.; Dolg, M.; Stoll, H.; Preuß, H., Energy-adjusted ab initio pseudopotentials for the second and third row transition elements. *Theoret. Chim. Acta* **1990**, *77* (2), 123-141.

[20] Tomasi, J.; Mennucci, B.; Cammi, R., Quantum Mechanical Continuum Solvation Models. *Chem. Rev.* **2005**, *105* (8), 2999-3094.

[21] Mitoraj, M.; Michalak, A., Natural orbitals for chemical valence as descriptors of chemical bonding in transition metal complexes. *J. Mol. Model.* **2007**, *13* (2), 347-355.

[22] Mitoraj, M. P.; Michalak, A.; Ziegler, T., A Combined Charge and Energy Decomposition Scheme for Bond Analysis. *J. Chem. Theory Comput.* **2009**, *5* (4), 962-975.

[23] Lenthe, E. v.; Baerends, E. J.; Snijders, J. G., Relativistic regular two-component Hamiltonians. *J. Chem. Phys.* **1993**, *99* (6), 4597-4610.

[24] Lenthe, E. v.; Baerends, E. J.; Snijders, J. G., Relativistic total energy using regular approximations. *J. Chem. Phys.* **1994**, *101* (11), 9783-9792.

[25] Becke, A. D., Density-functional exchange-energy approximation with correct asymptotic behavior. *Phys. Rev. A* **1988**, *38* (6), 3098-3100.

[26] Perdew, J. P., Density-functional approximation for the correlation energy of the inhomogeneous electron gas. *Phys. Rev. B* **1986**, *33* (12), 8822-8824.

conductor-like screening model (COSMO)[15] using the Turbomole package, version 6.6[28,29,30]) UV-vis and ^{13}C NMR computations were performed. The former (UV-vis) employed time-dependent DFT (TDDFT) with G09. The B3LYP[31,32,33,34] global hybrid functional and the range-separated CAM-B3LYP[35,36] functional that was designed to suitably describe the excited states with charge-transfer character were used in these computations along with the TZVP basis set and the PCM approach. The calculations covered the 100 lowest singlet excited states for each system. The simulated spectra shown are the sums of Gaussian functions centered at the vertical excitation energies and scaled using the calculated oscillator strengths, with a parameter of $\sigma = 0.15$ eV applied for the root mean square width. The latter calculations (^{13}C NMR) were performed with ADF2016 using both gradient (revPBE[8,37]) and global hybrid (B3LYP, PBE0[38]) density functionals, TZ2P / QZ4P (quadruple-ζ basis set with four sets of polarization functions) for C, N / Pt atoms, along with dichloromethane COSMO model, and employing ZORA to incorporate scalar and spin-orbit coupling[39] relativistic effects. As a reference tetramethylsilane (TMS) molecule was used. For a comparison, analogical NMR calculations were also performed for two freely optimized $[Pt(CN)_4]^{2-}$/HAT(CN)$_6$ clusters ($[Pt(CN)_4]^{2-}$:HAT(CN)$_6$ = 1:1) and their pristine components, $[Pt(CN)_4]^{2-}$ and HAT(CN)$_6$. In this subset of computations, acetonitrile COSMO model was employed to match experimental conditions of the NMR measurements.

Additional calculated data

Table S7 $[Pt(CN)_4]^{2-}$/TCP interaction energy components (in kcal·mol^{-1}) for structures **1-3** as obtained using the ETS energy decomposition scheme. For comparison the corresponding $[PtCl_4]^{2-}$/TCP interaction energy terms for the $(Pr_4N)_2[PtCl_4]$·TCP compound **R** along with

System	ΔE_{tot}	ΔE_{orb}	ΔE_{steric}	ΔE_{Pauli}	ΔE_{elstat}	ΔE_{disp}
R	-58.00	-36.05	-16.53	14.75	-31.29	-5.42
R$^{[Pt(CN)4]2-}$	-35.57	-15.54	-14.58	13.23	-27.81	-5.44
1	-33.85	-13.74	-12.38	10.64	-23.02	-7.73
2	-29.98	-16.96	-10.71	12.74	-23.45	-2.31
3^{I}	-28.16	-13.57	-12.56	6.39	-18.96	-2.02
3^{II}	-29.39	-16.10	-9.52	8.04	-17.56	-3.77

---

[27] Perdew, J. P., Erratum: Density-functional approximation for the correlation energy of the inhomogeneous electron gas. *Phys. Rev. B* **1986**, *34* (10), 7406.

[28] TURBOMOLE V6.6 2014, a development of University of Karlsruhe and Forschungszentrum Karlsruhe GmbH, 1989-2007, TURBOMOLE GmbH, since 2007; available from http://www.turbomole.com.

[29] Ahlrichs, R.; Bär, M.; Häser, M.; Horn, H.; Kölmel, C., Electronic structure calculations on workstation computers: The program system turbomole. *Chem. Phys. Lett.* **1989**, *162* (3), 165-169.

[30] Furche, F.; Ahlrichs, R.; Hättig, C.; Klopper, W.; Sierka, M.; Weigend, F., Turbomole. *WIREs Comput. Mol. Sci.* **2014**, *4* (2), 91-100.

[31] Becke, A. D., Density-functional thermochemistry. III. The role of exact exchange. *J. Chem. Phys.* **1993**, *98* (7), 5648-5652.

[32] Lee, C.; Yang, W.; Parr, R. G., Development of the Colle-Salvetti correlation-energy formula into a functional of the electron density. *Phys. Rev. B* **1988**, *37* (2), 785-789.

[33] Vosko, S. H.; Wilk, L.; Nusair, M., Accurate spin-dependent electron liquid correlation energies for local spin density calculations: a critical analysis. *Can. J. Phys.* **1980**, *58* (8), 1200-1211.

[34] Stephens, P. J.; Devlin, F. J.; Chabalowski, C. F.; Frisch, M. J., Ab Initio Calculation of Vibrational Absorption and Circular Dichroism Spectra Using Density Functional Force Fields. *J. Phys. Chem.* **1995**, *98* (45), 11623-11627.

[35] Yanai, T.; Tew, D.; Handy, N., A new hybrid exchange–correlation functional using the Coulomb-attenuating method (CAM-B3LYP). *Chem. Phys. Lett.* **2004**, *393* (1-3), 51-57.

[36] Autschbach, J.; Srebro, M., Delocalization Error and “Functional Tuning” in Kohn–Sham Calculations of Molecular Properties. *Acc. Chem. Res.*, 2014, *47* (8), 2592-2602.

[37] Zhang, Y.; Yang, W., Comment on “Generalized Gradient Approximation Made Simple”. *Phys. Rev. Lett.* **1998**, *80* (4), 890.

[38] Adamo, C.; Barone, V., Toward reliable density functional methods without adjustable parameters: The PBE0 model. *J. Chem. Phys.* **1999**, *110* (13), 6158-6170.

[39] van Lenthe, E.; Snijders, J. G.; Baerends, E. J., The zero-order regular approximation for relativistic effects: the effect of spin–orbit coupling in closed shell molecules. *J. Chem. Phys.* **1996**, *105* (15), 6505-6516.

$[Pt(CN)_4]^{2-}$/TCP interaction energy terms for the hypothetical $(Pr_4N)_2[Pt(CN)_4]{\cdot}TCP$ system $\mathbf{R}^{[Pt(CN)4]2-}$ are listed. PBE-D3/TZ2P ZORA calculations. $\mathbf{3}^{\mathbf{I}}$ / $\mathbf{3}^{\mathbf{II}}$ corresponds to ‘TCP perpendicular’ / ‘TCP parallel’ motifs present in **3**.

Table S8 Cation-cation dispersion interaction energy component (in kcal·mol^{-1}) for selected embrace motifs found in structures **1-3** as obtained using the ETS energy decomposition scheme. PBE-D3/TZ2P ZORA calculations.

System	Contact	ΔE_{disp}
1	DPE	-7.83
	PQPE	-7.74
	TQPE	-10.39
2	PQPE	-6.88
	SPE	-13.49
	SPE’	-10.62
3	PQPE	-11.03
	SPE	-16.69

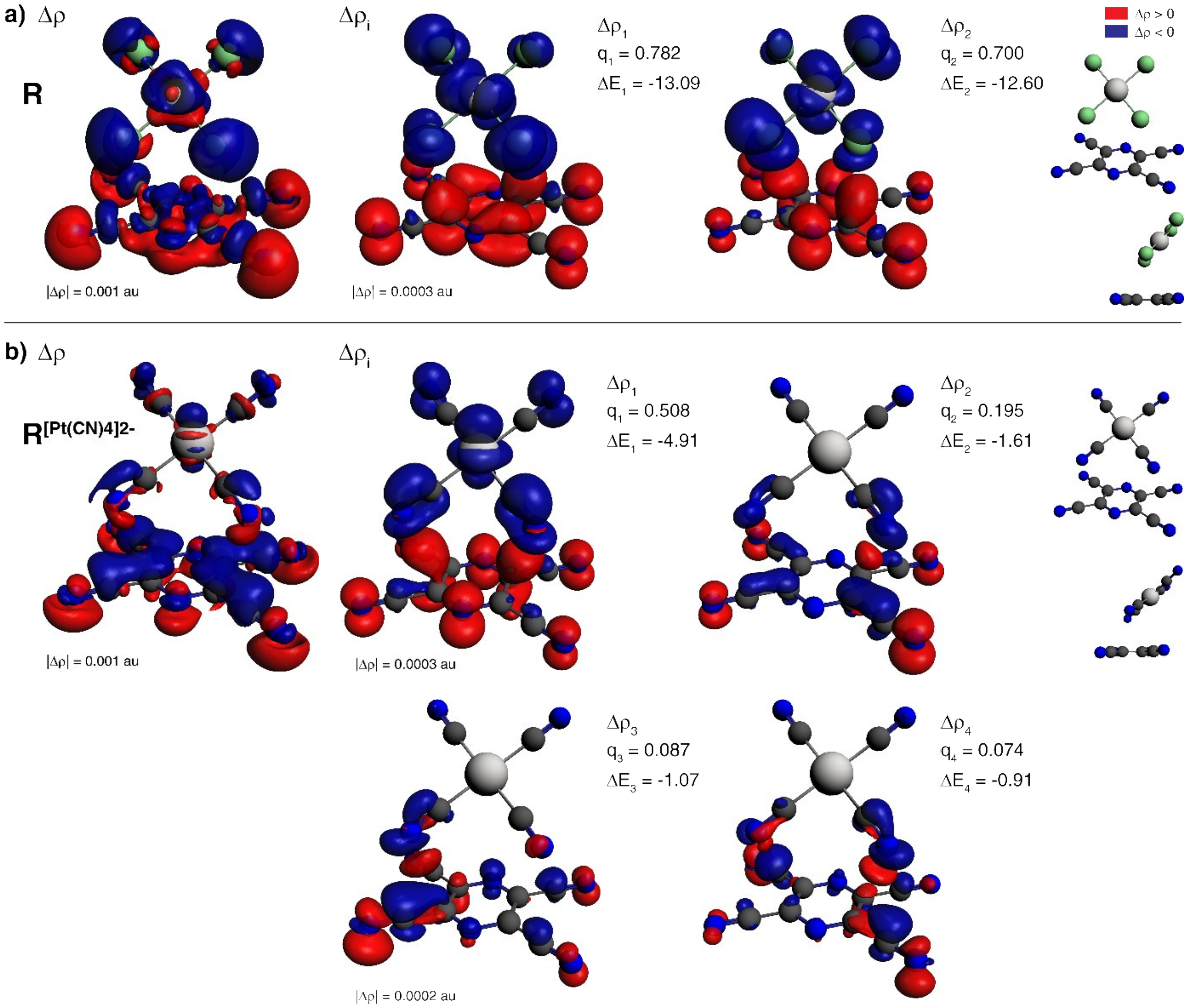

Figure S20 ETS-NOCV analysis of the interaction between TCP and Pt^{II} complex in the molecular clusters extracted from the $(Pr_4N)_2[PtCl_4]\cdot TCP$ compound **R** (panel a) and from the hypothetical $(Pr_4N)_2[Pt(CN)_4]\cdot TCP$ system **R**$^{\mathbf{[Pt(CN)4]2-}}$ (panel b). Isosurfaces of charge deformation (differential) density $\Delta\rho$ and dominant NOCV contributions to $\Delta\rho$ along with the corresponding charge (q) and orbital energy (ΔE in kcal·mol^{-1}) measures. Red / blue indicates inflow (gain) / outflow (loss) of electron density. PBE-D3/TZ2P ZORA calculations.

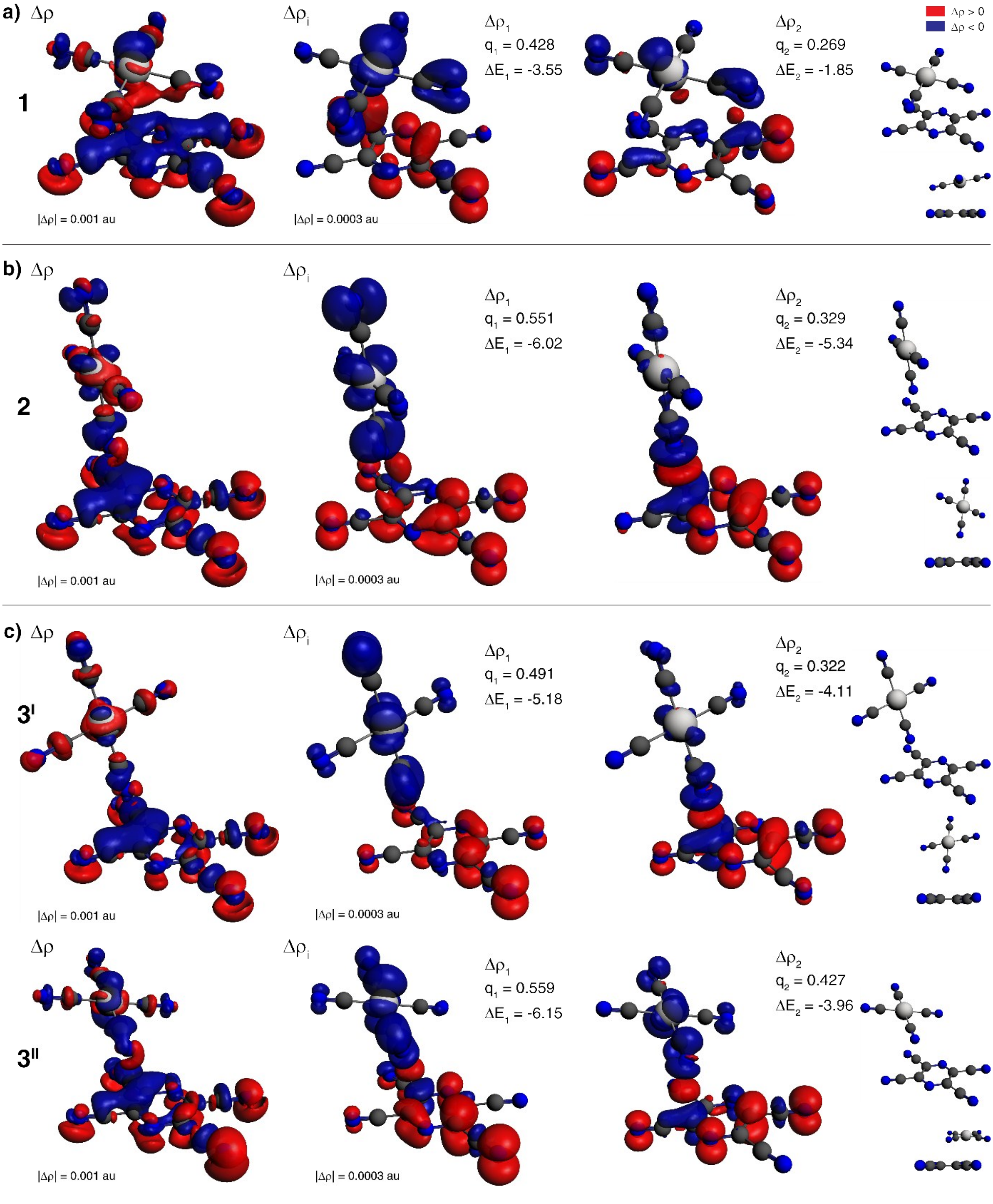

Figure S21 ETS-NOCV analysis of the interaction between TCP and $[Pt(CN)_4]^{2-}$ in the molecular clusters extracted from the structures **1**-**3**. Isosurfaces of charge deformation (differential) density $\Delta\rho$ and dominant NOCV contributions to $\Delta\rho$ along with the corresponding charge (q) and orbital energy (ΔE in kcal·mol^{-1}) measures. Red / blue indicates inflow (gain) / outflow (loss) of electron density. PBE-D3/TZ2P ZORA calculations.

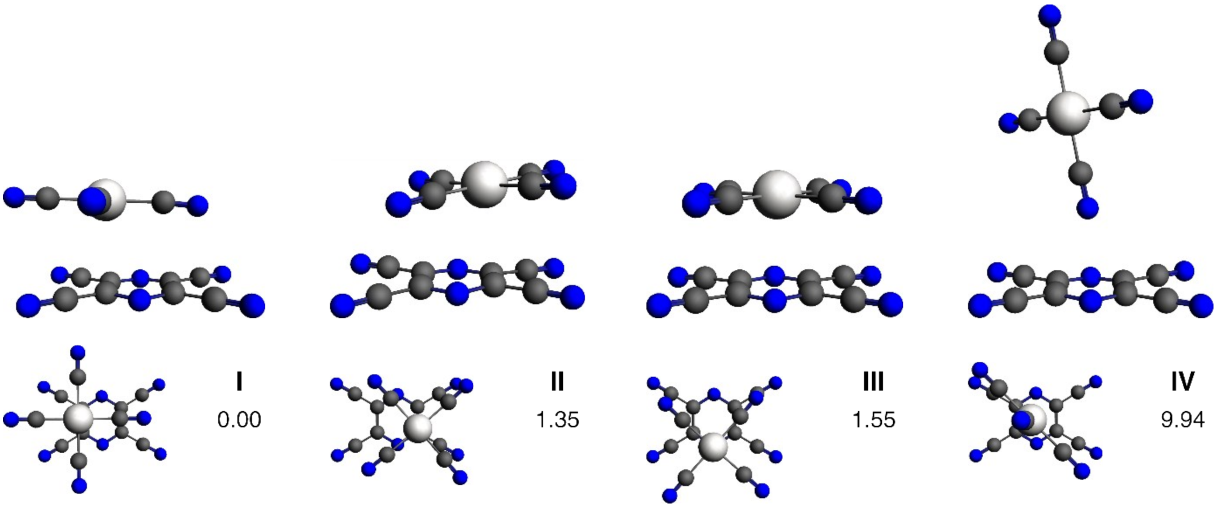

Figure S22 Selected optimized molecular structures of $[Pt(CN)_4]^{2-}$ + TCP system. Values listed are relative energy, in kcal·mol^{-1}. BP-D3/SVP COSMO(dichloromethane) calculations. In the article (see Figure 3), I / IV is referred to as ∥ / ⊥.

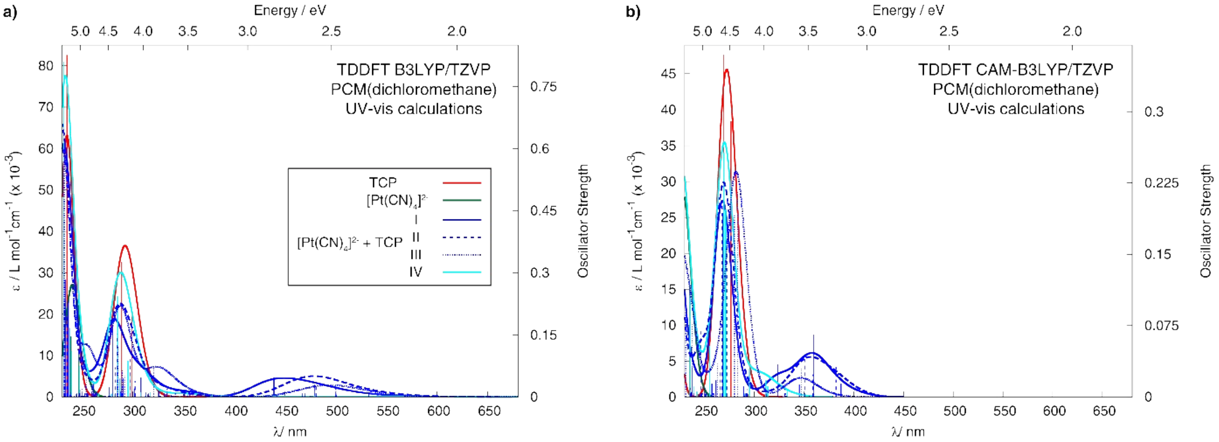

Figure S23 Simulated UV-vis spectra of $[Pt(CN)_4]^{2-}$ + TCP system and of the corresponding pristine fragments, i.e. $[Pt(CN)_4]^{2-}$ and TCP molecules. No spectral shift has been applied. Calculated excitation energies and oscillator strengths indicated as 'stick' spectra.

Table S9 Lowest-energy dominant excitations and occupied (occ) – unoccupied (unocc) MO pair contributions (greater than 10%) of $[Pt(CN)_4]^{2-}$ + TCP system I and IV based on TDDFT CAM-B3LYP/TZVP with dichloromethane continuum solvent model calculations.

Excitation	*E* / eV	λ / nm	*f*	occ no.	unocc no.	%
			I			
1	3.20	387	0.014	81	82	95.1
2	3.45	360	0.066	81	83	92.7
4	3.59	345	0.013	80	82	91.8
			IV			
1	3.72	333	0.005	79	82	90.4
3	3.95	314	0.011	78	82	54.5
				79	83	23.2
4	3.98	312	0.018	79	83	61.8
				78	82	22.5
7	4.20	295	0.030	78	83	65.6
				75	83	17.7

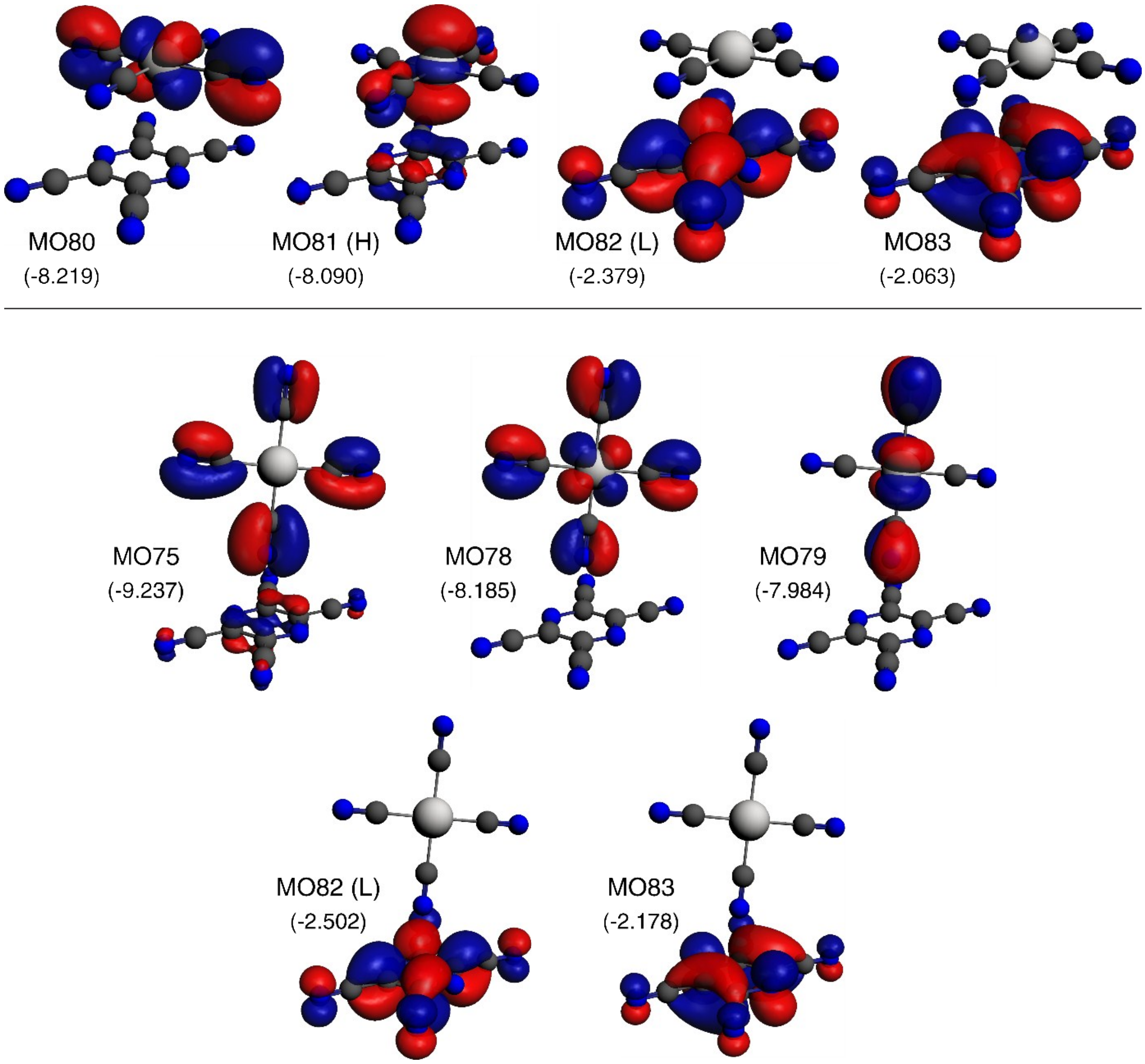

Figure S24 Isosurfaces (±0.03 au) of MOs involved in selected transitions of $[Pt(CN)_4]^{2-}$ + TCP system I (panel a) and IV (panel b) based on TDDFT CAM-B3LYP/TZVP with dichloromethane continuum solvent model calculations. ‘H’ = HOMO, ‘L’ = LUMO. Values listed in the parentheses are the corresponding orbital energies, in eV. Note that for the system IV HOMO (corresponding to a pure d_{z^2} Pt lone-pair orbital) is not presented as it is not involved in relevant excitations.

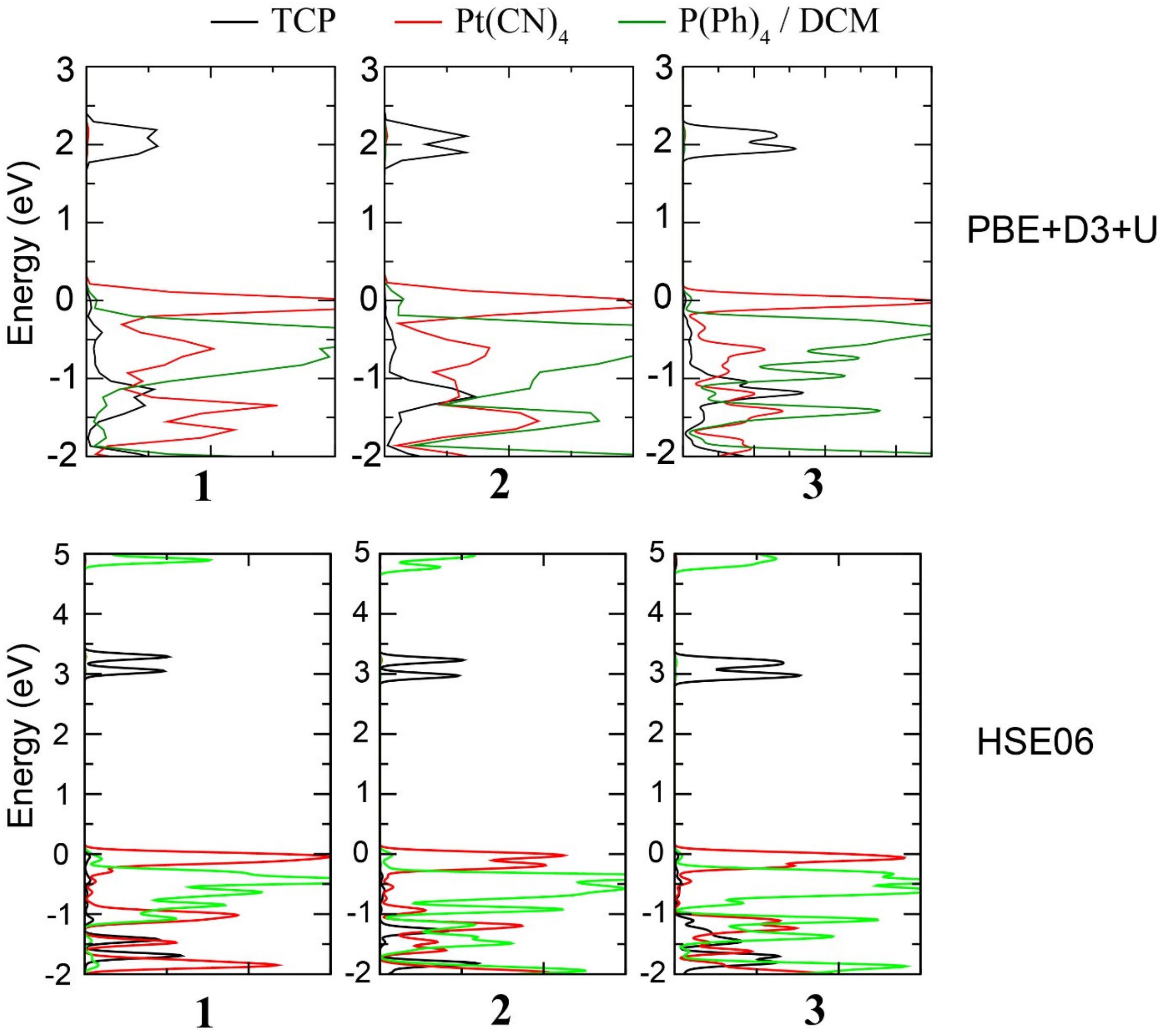

Figure S25 Computed electronic densities of states (DOS) of **1**, **2**, and **3** with (top) the PBE+D3+U functional, and (bottom) the HSE06 functional. The DOS plots are decomposed onto the molecular fragments, the valence band maximum is set to zero on the energy scale, and electronic smearing was applied to improve visibility.

Table S10 ^{13}C NMR chemical shifts calculated for $[Pt(CN)_4]^{2-}$ + TCP system I-IV (see **Figure S22**) and the corresponding pristine fragments, i.e. $[Pt(CN)_4]^{2-}$ and TCP molecules, in dichloromethane, with respect to the TMS signal. [a]

Method	^{13}C NMR δ_{iso} with respect to TMS [ppm]														
	C_{ext}					$C_{nitrile}$					$C_{CN\text{-}Pt}$				
	TCP	I	II	III	IV	TCP	I	II	III	IV	salt	I	II	III	IV
revPBE/SC	138.6	137.7	136.3	138.6	139.1	121.3	121.8	121.7	121.7	121.6	147.9	148.7	147.8	148.5	147.2
B3LYP/SC	145.1	145.0	144.0	145.8	145.7	123.2	123.6	123.4	123.4	123.5	156.5	156.7	155.9	149.5	155.8
PBE0/SC	144.7	144.5	144.5	145.3	145.1	124.5	124.9	124.9	124.7	124.8	157.9	157.8	157.8	157.9	157.2
revPBE/SO	138.9	138.0	137.2	139.4	139.4	122.0	122.6	122.4	122.4	122.2	134.4	135.4	134.7	135.1	133.8
B3LYP/SO	145.5	145.2	144.4	146.1	146.0	123.8	124.3	124.1	124.1	124.1	137.4	137.8	137.3	137.7	136.9
PBE0/SO	145.0	144.7	144.0	145.5	145.4	125.1	125.6	125.4	125.4	125.4	139.0	139.0	138.5	139.1	138.5
Expt.	134.54	Pt-TCP (fresh): 134.64 Pt-TCP (after 24h): 134.64				110.72	Pt-TCP (fresh): 111.00 (av.) Pt-TCP (after 24h): 110.98				122.28	Pt-TCP (fresh): 122.31 Pt-TCP (after 24h): 122.13 (av.)			

[a] In ppm. $\delta_{iso}(C) = \sigma_{iso}(C_{TMS}) - \sigma_{iso}(C)$; averaged values are listed. SC /SO = scalar / spin-orbit ZORA method. Experimental data based on **Figure S18** and **Table S5**.

Table S11 ^{13}C NMR chemical shifts calculated for $[Pt(CN)_4]^{2-}$ + TCP system I-IV (see **Figure S22**) and the corresponding pristine fragments, i.e. $[Pt(CN)_4]^{2-}$ and TCP molecules, in dichloromethane, with respect to the $C_{nitrile}$ signal of the pristine TCP. Note that the best agreement with the experimental data for the precursors was obtained using B3LYP/SO method (highlighted in orange).[a]

Method	^{13}C NMR δ_{iso} with respect to $-CN_{TCP}$ [ppm]														
	C_{ext}					$C_{nitrile}$					$C_{CN\text{-}Pt}$				
	TCP	I	II	III	IV	TCP	I	II	III	IV	salt	I	II	III	IV
revPBE/SC	17.24	16.31	15.00	17.30	17.74	0.00	0.50	0.40	0.35	0.26	26.54	27.34	26.45	27.12	25.83
B3LYP/SC	21.97	21.84	20.85	22.64	22.55	0.00	0.39	0.28	0.25	0.34	33.33	33.54	32.78	26.32	32.62
PBE0/SC	20.20	20.03	20.03	20.83	20.66	0.00	0.39	0.39	0.24	0.33	33.47	33.36	33.36	33.38	32.75
revPBE/SO	16.92	16.06	15.18	17.37	17.41	0.00	0.57	0.39	0.42	0.24	12.38	13.45	12.75	13.16	11.83
B3LYP/SO	21.67	21.42	20.58	22.27	22.24	0.00	0.47	0.35	0.35	0.32	13.63	14.00	13.47	13.95	13.11
PBE0/SO	19.91	19.62	18.86	20.45	20.36	0.00	0.47	0.33	0.33	0.31	13.91	13.91	13.44	14.00	13.39
Expt.	23.82	Pt-TCP (fresh): 23.92 Pt-TCP (after 24h): 23.92				0.00	Pt-TCP (fresh): 0.28 (av.) Pt-TCP (after 24h): 0.26				11.56	Pt-TCP (fresh): 11.59 Pt-TCP (after 24h): 11.41 (av.)			

[a] In ppm. $\delta_{iso}(C) = \delta_{iso}(C) - \delta_{iso}(C_{nitrile,\ TCP}) = \sigma_{iso}(C_{nitrile,\ TCP}) - \sigma_{iso}(C)$; averaged values are listed. SC /SO = scalar / spin-orbit ZORA method. Experimental data based on **Figure S18** and **Table S5**.

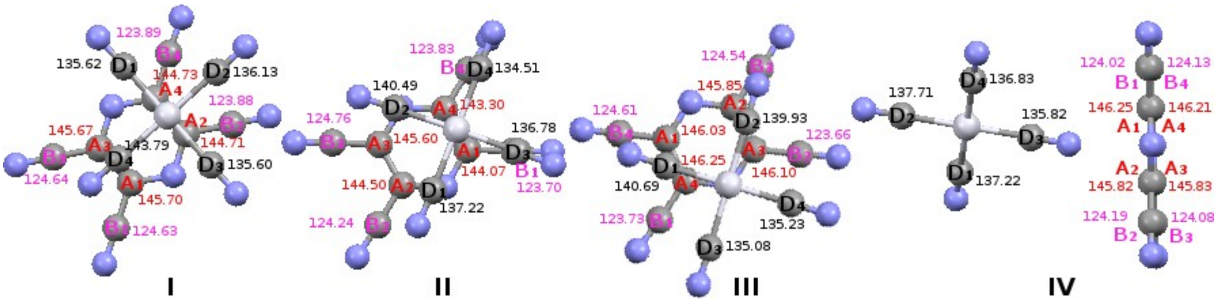

Figure S26 ^{13}C NMR chemical shifts, in ppm, calculated with B3LYP/SO for particular carbon atoms in $[Pt(CN)_4]^{2-}$ + TCP system I-IV, in dichloromethane, with respect to the TMS signal. Compare with **Table S12** and **Table S13**.

Table S12 ^{13}C NMR chemical shifts, in ppm, calculated with B3LYP/SO for $[Pt(CN)_4]^{2-}$ + TCP system I-IV and the corresponding pristine fragments, i.e. $[Pt(CN)_4]^{2-}$ and TCP molecules, in dichloromethane, with respect to the TMS signal. Compare with **Figure S26**.

C atom		TCP or salt	I	II	III	IV	Expt.
C_{ext}	A1	145.5	145.7	144.1	146.0	146.3	TCP: 134.54 Pt-TCP (fresh): 134.64 Pt-TCP (after 24h): 134.64
	A2		144.7	144.5	145.9	145.8	
	A3		145.7	145.6	146.1	145.8	
	A4		144.7	143.3	146.3	146.2	
	average		145.2	144.4	146.1	146.0	
$C_{nitrile}$	B1	123.8	124.6	123.7	123.7	124.0	TCP: 110.72 Pt-TCP (fresh): 111.00 (av.) Pt-TCP (after 24h): 110.98
	B2		123.9	124.2	123.7	124.2	
	B3		124.6	124.8	124.5	124.1	
	B4		123.9	123.8	124.6	124.1	
	average		124.3	124.1	124.1	124.1	
$C_{CN\text{-}Pt}$	D1	137.4	135.6	137.2	140.7	137.2	salt: 122.28 Pt-TCP (fresh): 122.31 Pt-TCP (after 24h): 122.13 (av.)
	D2		136.1	140.5	139.9	137.7	
	D3		135.6	136.8	135.1	135.8	
	D4		143.8	134.5	135.2	136.8	
	average		137.8	137.3	137.7	136.9	

Table S13 ^{13}C NMR chemical shifts, in ppm, calculated with B3LYP/SO for $[Pt(CN)_4]^{2-}$ + TCP system I-IV, in dichloromethane, with respect to the particular signals of the corresponding pristine fragments, i.e. $[Pt(CN)_4]^{2-}$ and TCP molecules. Compare with **Figure S26**.

C atom		TCP or salt	I	II	III	IV	Expt.
C_{ext}	A1	0.00	0.25	-1.38	0.58	0.80	TCP: 0.00 Pt-TCP (fresh): 0.10 Pt-TCP (after 24h): 0.10
	A2		-0.74	-0.95	0.40	0.37	
	A3		0.22	0.15	0.65	0.38	
	A4		-0.72	-2.15	0.80	0.76	
	average		-0.25	-1.08	0.61	0.58	
$C_{nitrile}$	B1	0.00	0.84	-0.09	-0.06	0.23	TCP: 0.00 Pt-TCP (fresh): 0.28 (av.) Pt-TCP (after 24h): 0.26
	B2		0.09	0.45	-0.13	0.41	
	B3		0.85	0.97	0.75	0.34	
	B4		0.10	0.04	0.82	0.29	
	average		0.47	0.35	0.35	0.32	
$C_{CN\text{-}Pt}$	D1	0.00	-1.79	-0.19	3.28	-0.19	salt: 0.00 Pt-TCP (fresh): 0.03 Pt-TCP (after 24h): -0.15 (av.)
	D2		-1.28	3.08	2.52	0.30	
	D3		-1.81	-0.63	-2.33	-1.59	
	D4		6.38	-2.90	-2.18	-0.58	
	average		0.38	-0.16	0.32	-0.52	

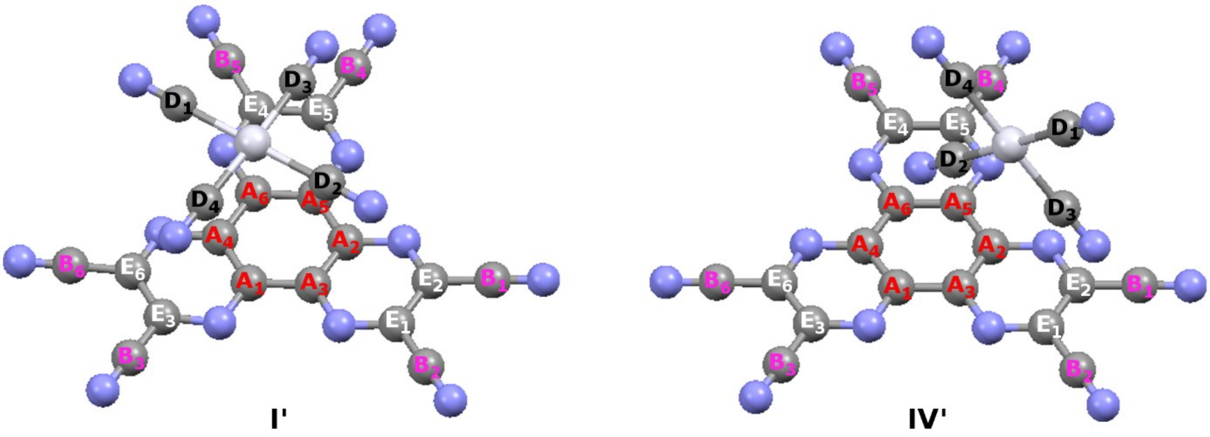

I'

ΔE = 0.00

IV'

ΔE = 11.16

Figure S27 Selected optimized molecular structures of $[Pt(CN)_4]^{2-}$ + HAT$(CN)_6$ system with atom labelling scheme used for the NMR analysis. Values listed are relative energy, ΔE, in kcal·mol^{-1}. BP-D3/SVP COSMO(acetonitrile) calculations. Compare with **Table S14** and **Table S15**.

Table S14 ^{13}C NMR chemical shifts, in ppm, calculated with B3LYP/SO for $[Pt(CN)_4]^{2-}$ + $HAT(CN)_6$ system I' and IV' (see **Figure S27**) and the corresponding pristine fragments, i.e. $[Pt(CN)_4]^{2-}$ and $HAT(CN)_6$ molecules, in acetonitrile, with respect to the TMS signal.

C atom		$HAT(CN)_6$ / salt	I'	IV'	Expt.
C_{int}	A1	153.5	152.1	154.1	$HAT(CN)_6$: 143.10 adduct: 143.33
	A2		153.6	153.1	
	A3		153.6	153.1	
	A4		152.6	154.4	
	A5		152.1	154.1	
	A6		152.6	154.5	
	average		152.8	153.9	
C_{ext}	E1	145.9	146.0	147.8	$HAT(CN)_6$: 136.38 adduct: 136.24
	E2		146.0	147.8	
	E3		147.5	145.1	
	E4		145.2	144.9	
	E5		147.5	145.2	
	E6		145.2	144.8	
	average		146.2	145.9	
$C_{nitrile}$	B1	126.2	126.1	126.6	$HAT(CN)_6$: 113.90 adduct: 114.02
	B2		126.1	126.5	
	B3		126.3	126.3	
	B4		126.3	126.3	
	B5		126.0	126.3	
	B6		126.0	126.3	
	average		126.1	126.4	
$C_{CN\text{-}Pt}$	D1	137.9	134.7	137.7	salt: 122.48 adduct: 121.97 (av.)
	D2		135.8	139.6	
	D3		136.9	144.4	
	D4		136.8	137.4	
	average		136.1	139.8	

Table S15 ^{13}C NMR chemical shifts, in ppm, calculated with B3LYP/SO for $[Pt(CN)_4]^{2-}$ + $HAT(CN)_6$ system I' and IV' (see **Figure S27**), in acetonitrile, with respect to the particular signals of the corresponding pristine fragments, i.e. $[Pt(CN)_4]^{2-}$ and $HAT(CN)_6$ molecules.

C atom		$HAT(CN)_6$ / salt	I'	IV'	Expt.
C_{int}	A1	0.00	-1.46	0.52	$HAT(CN)_6$: 0.00 adduct: 0.23
	A2		0.11	-0.48	
	A3		0.09	-0.48	
	A4		-0.91	0.90	
	A5		-1.48	0.52	
	A6		-0.93	0.92	
	average		-0.76	0.32	
C_{ext}	E1	0.00	0.12	1.94	$HAT(CN)_6$: 0.00 adduct: -0.14
	E2		0.13	1.97	
	E3		1.63	-0.76	
	E4		-0.62	-0.99	
	E5		1.62	-0.71	
	E6		-0.62	-1.03	
	average		0.38	0.07	
$C_{nitrile}$	B1	0.00	-0.08	0.41	$HAT(CN)_6$: 0.00 adduct: 0.12
	B2		-0.08	0.39	
	B3		0.12	0.14	
	B4		0.11	0.13	
	B5		-0.16	0.18	
	B6		-0.15	0.17	
	average		-0.04	0.24	
$C_{CN\text{-}Pt}$	D1	0.00	-3.16	-0.15	salt: 0.00 adduct: -0.51 (av.)
	D2		-2.10	1.75	
	D3		-0.98	6.56	
	D4		-1.04	-0.53	
	average		-1.82	1.91	

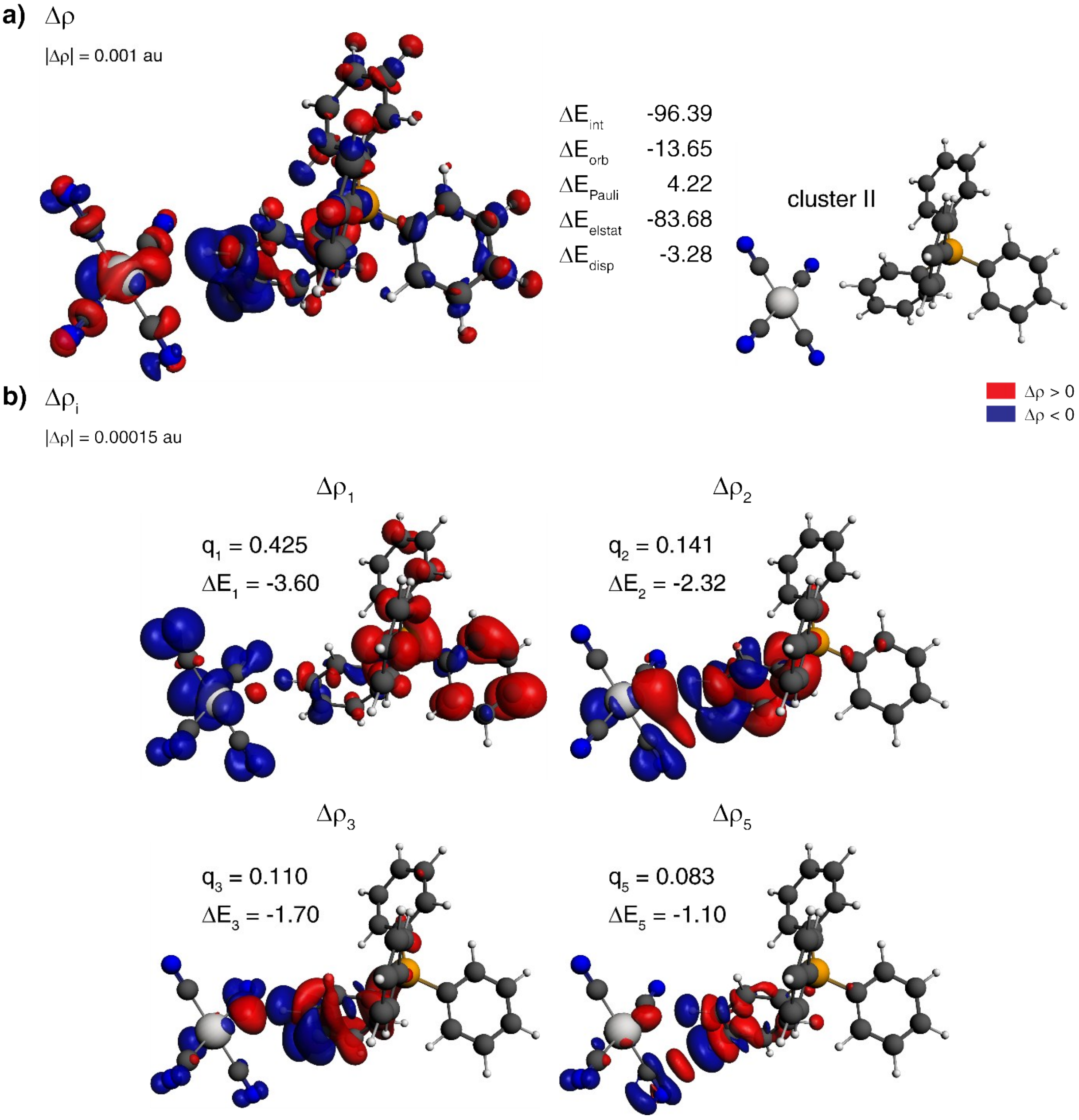

Figure S28 ETS-NOCV analysis of the interaction between PPh_4^+ and Pt^{II} complex in the molecular cluster II extracted from the $(PPh_4^+)_2[PtCl_4]\cdot H_2O$ salt. Isosurfaces of charge deformation (differential) density $\Delta\rho$ (panel a) and dominant NOCV contributions to $\Delta\rho$ along with the corresponding charge (q) and orbital energy (ΔE in kcal·mol^{-1}) measures (panel b). Red / blue indicates inflow (gain) / outflow (loss) of electron density. PBE-D3/TZ2P ZORA calculations.

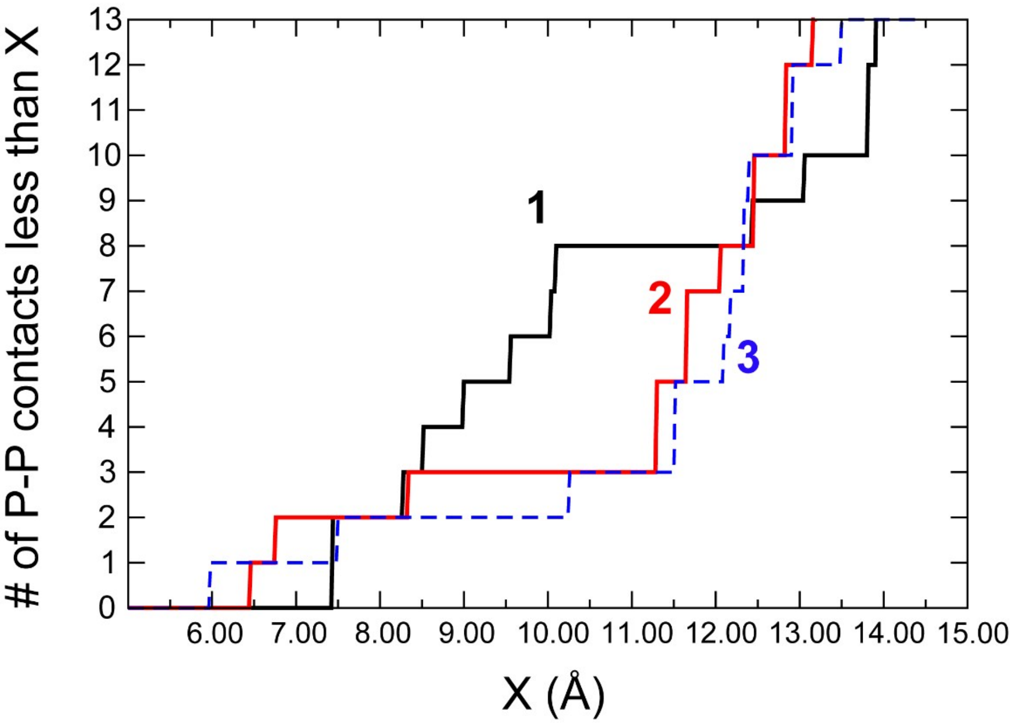

Figure S29 Plot of the number of PPh_4^+-PPh_4^+ contacts within a given radius of each PPh_4^+ cation in the PBE+D3+U optimized geometries of **1** (black solid line), **2** (red solid line), and **3** (blue dashed line). Note the shorter contact distances of the closest two contacts in **2**/**3** vs. **1**; these correspond with the SPE/PQPE types of "phenyl embrace" in **2**/**3** and the TQPE types in **1** (see **Table S8** for estimations of the stabilizing dispersion interactions between molecules within these motifs). Also note the general shift in the number of contact distances between 8.0 and 11.0 Å in **2**/**3** vs. **1**.